Title

Investigating the role of a Lamin A-OGT-Emerin axis in female stem cells

Permalink

https://escholarship.org/uc/item/5253m7nk

Author

Augspurger, Katherine Rose

Publication Date

2025

Peer reviewed|Thesis/dissertation

Investigating the role of a Lamin A-OGT-Emerin axis in female stem cells

by
Katherine Augspurger

DISSERTATION
Submitted in partial satisfaction of the requirements for degree of
DOCTOR OF PHILOSOPHY

in

Biochemistry and Molecular Biology

in the

GRADUATE DIVISION
of the
UNIVERSITY OF CALIFORNIA, SAN FRANCISCO

Approved:

DocuSigned by:

Danica Galonic Fujimori

Danica Galonic Fujimori
_____
82967A5AE18B4D6...
Chair

DocuSigned by:

Jeremy Reiter

Jeremy Reiter
_____
DocuSigned by: ...4B3...

Geeta Narlikar

Geeta Narlikar
_____
DocuSigned by: ...43B...

Barbara Panning

Barbara Panning
_____
Signed by: ...7C95417...

Abby Buchwalter

Abby Buchwalter
_____
399BB46C754548E...
Committee Members

Copyright 2025

by

Katherine Augspurger

Acknowledgements

I would not have made it to this point in my PhD without the help, support, love and encouragement of many people in my life.

First and foremost, I'd like to thank my advisors Abby Buchwalter and Barbara Panning. Through all the ups and downs of graduate school they have supported me and my education. They've allowed me the space to make mistakes and learn from them, and to succeed on my own and grow into the scientist I am today. I owe a lot of my successes to these two, and I'm thankful to have chosen them as my mentors.

In addition to Abby and Barbara, I also need to thank all my fellow lab members in the two labs over the years. This crew of "labbies" have celebrated the wins throughout my project, grieved with me during the losses, and made me the scientist I am today. I especially want to thank Yewande Alabi and Harold Marin, my fellow graduate students who started in the ABC lab at the same time. I feel incredibly lucky to have had such great friends and scientists to go through this crazy roller coaster ride with. I'd also Like to specifically thank my Panning lab big sister Betsy Martin for helping to guide me through my first few years as a grad student, and Luke Strauskulage for always being literally right behind me in the Panning lab and ready to listen or grab a beer when I needed someone to lean on. I'll also add a big thanks here to Jason Maynard and Kevin Welle for being fantastic and communicative collaborators.

Next, I'd like to thank Mary Porter. Mary took a chance on me during my first year at the University of Minnesota and gave me the opportunity to build my research skills early in my career. Along with Mary comes the other full-time members of the Porter Lab – Doug Tritschler and the late Kelly Bower who set me up to be the western blot

whiz that I am today. Additionally, I'd like to thank Wendy Gibbons for taking notice of my excitement for science back in high school and connecting me with Mary when I got to Minnesota. I would not have even considered going into a PhD program without Mary and Wendy.

Finally, a huge thank you to my friends and family that have given me the emotional support to make it to the finish line. To Haley Gause, Lili Kim, Liz Bond, and Henry Ng, Ady Steinbach, and Francesca Del Frate for giving me shoulders to lean on and the space to let loose and be myself. You all inspire me every day and I'm so happy to have you as my chosen family. To my sister Christine, who is always in my corner and ready to help me with big and little decisions whenever I need it. And the biggest thank you goes to my parents, Steve and Debbie Augspurger. They were the first people to encourage me to pursue what I was interested in and to challenge myself by exploring math and science. They have never stopped showing up for me and cheering me on, and I don't know where I would be without their amazing love and support.

Contributions

The text of chapter two of this thesis has been submitted as a preprint to *bioRxiv* and will be submitted for publication. It includes the following contributions from collaborators:

- The TMT mass spectrometry for Figure 2.2 A and C was performed by Kevin Welle in the lab of Dr. Sina Ghaemmaghami at the University of Rochester
- The cell culture for the SILAC experiment in Figure 2.2 B-E was done by Dr. Betsy Martin in the Panning lab.
- The SILAC mass spectrometry for Figure 2.2 B-E was performed by Dr. Jason Maynard in the lab of Dr. Alma Burlingame at UCSF

The TMT mass spectrometry in Chapter 5 was also performed by Kevin Welle at the University of Rochester, the cell culture for SILAC in Chapter 5 was done by Dr. Betsy Martin, and the SILAC mass spectrometry in Chapter 5 was performed by Dr. Jason Maynard in the lab of Dr. Alma Burlingame.

The RNAseq library prep in Chapters 4 and 5 was done by Michael Adkisson, Lenka Maliskova, and Walter Eckalbar at the Genomics CoLab at UCSF, and the sequencing was performed at the UCSF CAT. RNAseq analysis utilized scripts and pipelines previously written by Dr. Harold Marin and Karissa Hansen.

"I can break through the earth, come up soft and wild."

-Hayley Williams

Investigating the role of a Lamin A-OGT-Emerin axis in female stem cells

Katherine R. Augspurger

Abstract

Lamin A processing is highly regulated, and necessary for proper assembly of the nuclear lamina facilitating its role in nuclear structure and chromatin organization. Pre-lamin A is first farnesylated, and then a short c-terminal peptide is cleaved to produce mature lamin A. *O*-GlcNAc Transferase (OGT), a glucose sensitive post-translational modification enzyme, has been identified as a potential regulator of lamin A. To explore the role of OGT in lamin A biogenesis, we examined the effects of variation in OGT levels, small molecule inhibition of OGT, and measured tail cleavage efficiency. Mutation of an OGT binding site and *O*-GlcNAc sites reduced tail cleavage efficiency suggesting that *O*-GlcNAcylation promotes lamin A processing. However, variation in OGT dose or inhibition of its activity did not alter endogenous lamin A abundance and distribution and did not disrupt differentiation. Likewise, another X-linked gene product, emerin, interacts with lamin A and is *O*-GlcNAc modified. As the sole developmental difference between XX and XY mESCs is that XX mESC must undergo X-chromosome inactivation (XCI), high expression of X-linked gene products, like emerin, may aid in regulation of XCI. However, perturbations to emerin in XX mESCs do not cause changes in XCI or disrupt epiblast differentiation. These results

shed light onto the role of the nuclear lamina and lamin associate proteins in XCI. Additionally, our findings add to our understanding of the regulatory process behind lamin A cleavage and identify a potential link between glucose metabolism and lamina function.

Table of Contents

List of Figures

Chapter 1

Chapter 2

Chapter 3

Chapter 4

Chapter 5

Appendix

List of Tables

Appendix

Chapter 1

Introduction

The nuclear lamina and lamin A

The nuclear lamina is a protein meshwork that surrounds the nucleus in mammalian cells(Burke & Stewart, 2013; Gruenbaum & Foisner, 2015; Shin & J.Worman, 2021). It provides structure and rigidity to the nucleus, as well as helping to organize chromatin. It is made up of 4 individual lamin proteins: lamin A, lamin B1, lamin B2, and lamin C(Burke & Stewart, 2013; Gruenbaum & Foisner, 2015). Lamin B1 and B2 are transcribed from their respective genes, while lamin A and lamin C are splice isoforms of the same *lmna* gene(Burke & Stewart, 2013; Gruenbaum & Foisner, 2015). The lamins all have similar structure, with a long rod-like coil-coil domain, an Ig-fold like globular domain, and a C-terminal unstructured tail (Burke & Stewart, 2013; Gruenbaum & Foisner, 2015; Samson et al., 2018). The coil-coil domains aid in dimerization and polymerization into the larger intermediate filament proteins that make up the lamina meshwork (Burke & Stewart, 2013; Gruenbaum & Foisner, 2015). Each lamin isoform is expressed differentially between cell types. For example, lamin A is highly expressed in cardiac muscle cells but specifically degraded the central nervous system(Jung et al., 2012).

Post-translationally, each lamina component is processed uniquely. Lamin B1 and B2 are farnesylated, the terminal amino acid is cleaved, and then finally carboxy-methylated on the C-terminus(Burke & Stewart, 2013; Davies et al., 2009). Lamin A begins to be processed in the same way, but after carboxy methylation the protease ZMPSTE24 cleaves off the last 18 amino acids and the farnesyl group (Burke & Stewart, 2013; Davies et al., 2009). Conversely, lamin C does not undergo any post-translational processing(Burke & Stewart, 2013; Gruenbaum & Foisner, 2015). These

processing steps are highly regulated, and defects in processing can lead to disease(Burke & Stewart, 2013; Davies et al., 2009; Goldman et al., 2004; Gruenbaum & Foisner, 2015).

Diseases resulting from defects in the nuclear lamina are known as laminopathies. Mutations in lamin A are known to cause four types of laminopathies: striated muscle diseases, adipose tissue disease, peripheral neuropathy, and progeroid diseases(Goldman et al., 2004; Shin & J.Worman, 2021). Progeroid disorders are caused by defects in lamin A processing. Tthe most well-known progeroid disorders is Hutchinson-Gilford Progeria Syndrome (HGPS). In HGPS, a dominant negative point mutations causes the cell to recognize a cryptic splice site in the lamin A tail(Hamczyk et al., 2019; Kim et al., 2023). This alternative splicing event removes 50 amino acids surrounding the ZMPSTE cleavage point in lamin A, thus causing farnesylated but not cleaved lamin A to be incorporated into the nuclear lamina(Burke & Stewart, 2013; Goldman et al., 2004; Kim et al., 2023; Shin & J.Worman, 2021). In HGPS, the addition of farnesyl lamin A into the lamina results in deformed and blebbed nuclei(Goldman et al., 2004; Kim et al., 2023). As the disease progresses, HGPS patients develop occlusive cardiovascular disease that is typically the cause of death of patients in their teens(Hamczyk et al., 2019; Shin & J.Worman, 2021). However, the downstream molecular effects of farnesylated lamin A are not well understood. Studies have linked farnesyl lamin A to decreased viability and apoptosis, along with impaired DNA repair mechanisms, and overall genomic instability(Hamczyk et al., 2019; Kim et al., 2023).
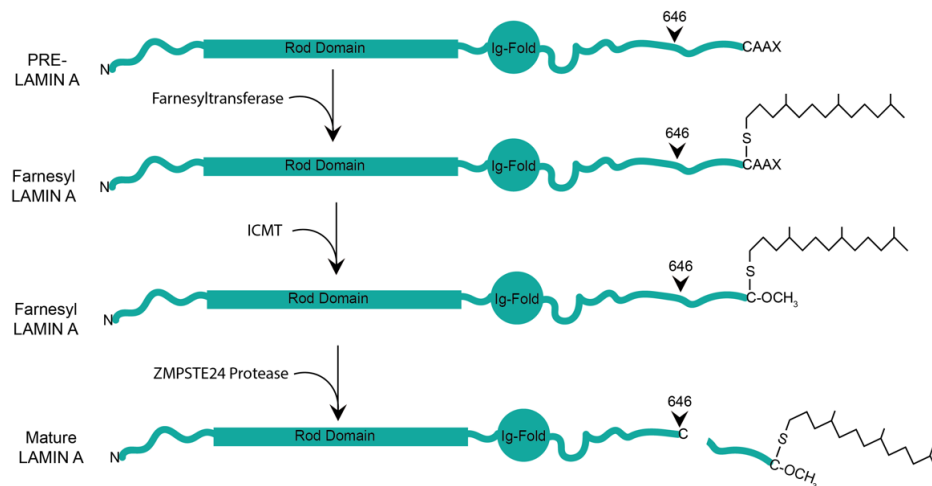
Figure 1.1 *Lamin A processing steps.* Lamin A is first translated as a pre-protein with a CAAX domain on the C-terminus. The CAAX is then farnesylated, and the -AAX is removed by FACE2 and carboxymethylated by ICMT. Finally, the last 18 amino acids and the farnesyl group are cleaved by ZMPSTE24, creating mature lamin A that can be correctly incorporated into the nuclear lamina.

O-GlcNAc Modification by OGT

Previous studies have connected lamin A with an X-linked metabolic regulator, *O*-GlcNAc-transferase (Simon et al., 2018). OGT is the singular enzyme that adds *O*-linked glycosylation modifications to Ser and Thr proteins in the cytoplasm, nucleus, and mitochondria(Bond & Hanover, 2015; Hart & Copeland, 2010; Levine & Walker, 2016). Its substrate, UDP-GlcNAc, is generated from the hexosamine biosynthetic pathway (HBP) (Bond & Hanover, 2015; Hart & Copeland, 2010; Levine & Walker, 2016). The HBP synthesizes UDP-GlcNAc from glucose, acetyl-CoA, ATP, glutamine, and uridine – linking *O*-GlcNAcylated proteins to each of the metabolic pathways of these components(Bond & Hanover, 2015; Hart & Copeland, 2010; Levine & Walker, 2016) (Figure 1.2). Specifically, overall levels of *O*-GlcNAcylation directly correlate with glucose levels in cell culture conditions(Stephen et al., 2021; Walgren et al., 2003). *O*-

GlcNAc modifications are typically found in intrinsically disordered regions of proteins similarly to phosphorylation(Bond & Hanover, 2015). Studies have shown that perturbations to *O*-GlcNAcylation levels also frequently affect phosphorylation stoichiometry(Bond & Hanover, 2015; Levine & Walker, 2016). Removal of *O*-GlcNAcylation is performed by the single enzyme, *O*-GlcNacase (OGA). OGA is autosomal and is the sole enzyme that removes *O*-GlcNAc modifications(Bond & Hanover, 2015; Stephen et al., 2021).

   O-GlcNacylation has been identified as a regulator of many pathways in the cell. In the catalytic domain of TET1, *O*-GlcNAc modifications increase the activity of TET1, thus decreasing DNA methylation in the nucleus(Hrit et al., 2018). Additionally, it has been reported that *O*-GlcNAcylation may inactivate AKT, a Ser/Thr protein kinase involved in several signaling cascades (Bond & Hanover, 2015; Hart & Copeland, 2010; Levine & Walker, 2016). Another well-known *O*-GlcNAc modified family of proteins are nucleoporins. Many nuclear pore complex (NPC) proteins are *O*-GlcNAcylated which is thought to aid in allowing larger proteins to enter the nucleus through the NPC(Bond & Hanover, 2015; Levine & Walker, 2016).
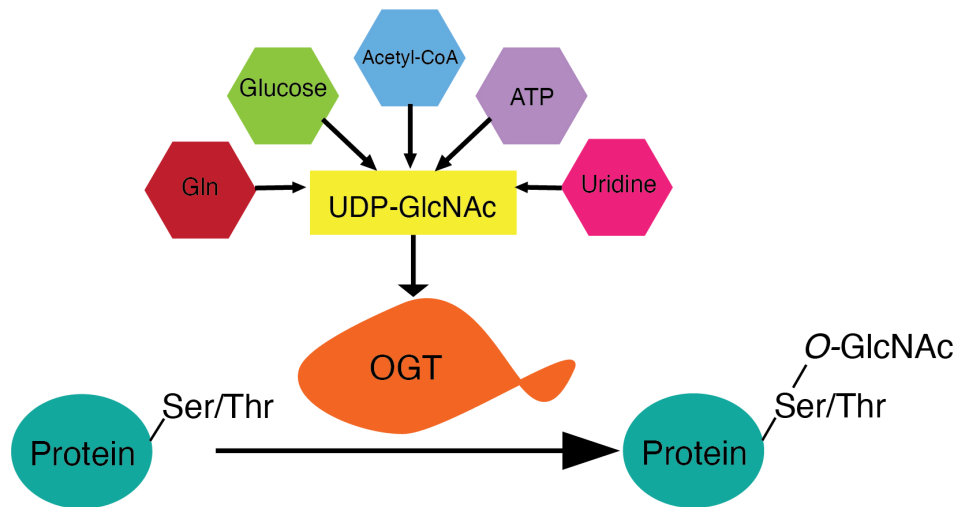
Figure 1.2 *OGT utilizes UDP-GlcNAc to modify proteins.* UDP-GlcNAc is synthesized via the hexosamine biosynthetic pathway and then added to Ser and Thr residues on proteins with an *O*-link by OGT.

Emerin

Another X-lined protein that has been linked to lamin A is emerin. Emerin is in the LEM (LAP2, Emerin, MAN1) family of proteins which all contain a LEM domain and interact with the nuclear lamina (Berk, Tifft, et al., 2013; Berk et al., 2014). Lamin A is required for proper localization of emerin at the nuclear periphery(Burke & Stewart, 2013). Emerin has been linked to many pathways in the cell including membrane trafficking, wnt signaling, and musculoskeletal development(Koch & Holaska, 2014; Östlund et al., 1999). However, emerin knockout mice survive into adulthood with minimal negative phenotypes, suggesting that the function of emerin is redundant in mice(Ozawa et al., 2006).

The structure of emerin gives little insight into its role in the cell. Emerin contains an N-terminal transmembrane domain, a long unstructured domain, and a LEM domain

on the C-terminus(Lee et al., 2001). Emerin is mostly localized to the inner nuclear membrane (INM), though it also moves through the endoplasmic reticulum (ER) (Berk, Tifft, et al., 2013; Berk et al., 2014). The transmembrane domain of emerin connects the protein to the INM and the ER membrane, while the unstructured domain and LEM domain have been reported to interact with lamin A(Lee et al., 2001). In complex with barrier-to-autointegration-factor-1(BAF) and the lamin A Ig-fold, emerin's LEM domain interacts with chromatin at the nuclear periphery, suggesting that emerin may play a role in peripheral heterochromatin silencing(Berk et al., 2014; Oca et al., 2005; Samson et al., 2018).

Mutations in emerin can also cause striated muscle diseases. The most well-known emerin-related disease is Emery-Dryfuss Muscular Dystrophy (EDMD)(Berk, Tifft, et al., 2013; Koch & Holaska, 2014). EDMD can be caused by both lamin A and emerin mutations, the only difference being the X-linked inheritance pattern of emerin based EDMD(Koch & Holaska, 2014; Shin & J.Worman, 2021). The mutations in emerin that lead to X-linked EDMD usually cause an effective loss of emerin protein at the nuclear periphery(Koch & Holaska, 2014). Unlike mice, which are generally unaffected by emerin loss (Ozawa et al., 2006), the human disease phenotype of EDMD can be severe – causing joint issues, muscle weakness, and cardiomyopathy (Koch & Holaska, 2014; Shin & J.Worman, 2021).

Stem Cells and XCI

In this study, we primarily employed mouse embryonic stem cells (mESCs). mESCs originate from the inner cell mass at the blastocyst stage of embryonic

development (Evans & Kaufman, 1981; G. R. Martin, 1981). At this stage, XX mESCs have not undergone X-chromosome inactivation (Maduro et al., 2016). With two active X chromosomes (Xs), the XX mESCs produce a higher dosage of X-linked gene products(Schulz et al., 2014), including OGT and emerin, compared to XY mESCs. The high abundance OGT and emerin make the XX and XY mESCs an ideal system to study natural variation in the abundance of these proteins.

At approximately embryonic day 5.5, XX mESCs undergo XCI(Maduro et al., 2016). XCI is the process by which XX mESCs normalize their X-linked gene dosage in comparison to XY mESCs. XCI is characterized by a series of steps that compact and silence the inactive X chromosome (Xi). Xist RNA is transcribed and coats the Xi along with H3K27me3 to signal for silencing(Maduro et al., 2016). Additionally, the Xi is positioned close to the nuclear periphery and is thought to interact with lamin B receptor at the nuclear periphery(Chen et al., 2016, 2017; Wang et al., 2017).

Summary

The dynamic relationship between lamin A, OGT, and emerin leads to questions surrounding the relationships between them. In Chapters 2 and 3, the regulatory function of *O*-GlcNAcylated lamin A is explored, while the function of lamin A during differentiation in XX mESCs is studied further in Chapter 4. Finally, the function of emerin both before and after differentiation is explored in Chapter 5. Dissecting the function of these three proteins alone and in combination will provide insight into the complex regulatory systems of mammalian cells during development and aging.

Chapter 2

O-GlcNAc modifications regulate lamin A tail processing

Introduction

Lamin A is one component of the nuclear lamina, a protein meshwork that surrounds the nucleus(Burke & Stewart, 2013; Gruenbaum & Foisner, 2015). The lamina connects the inner nuclear membrane to chromatin and performs two functions: providing physical rigidity to dampen external forces on the nucleus and scaffolding chromatin to influence DNA-templated processes(Gruenbaum & Foisner, 2015). Mutations in the nuclear lamina can lead to disease, including progeroid disorders that are characterized by rapidly advancing cardiovascular disease(Davies et al., 2009; Shin & J.Worman, 2021).

The components of the nuclear lamina can be separated into two groups, the A-type and B-type Lamins. B-type Lamins are transcribed from their respective *LMNB1* and *LMNB2* genes, while A-type Lamins, lamin A and lamin C, are splice isoforms of the *LMNA* gene(Burke & Stewart, 2013; Davies et al., 2009). Uniquely, lamin A must be processed before it can be incorporated into the nuclear lamina. Mutations that perturb this processing cause Hutchinson-Gilford progeria syndrome (Burke & Stewart, 2013; Davies et al., 2009).

Lamin A processing and localization is a multi-step process. The lamin A tail is first farnesylated at a C-terminal CAAX motif, which is thought to promote association with the nuclear membrane. A C-terminal peptide is then cleaved at tyrosine 646 (Y646) by the protease ZMPSTE24(Burke & Stewart, 2013; Davies et al., 2009), removing the last 18 residues and the farnesylated CAAX to produce mature lamin A. A mutation that results in a loss of 50 residues around Y646 causes accumulation of farnesylated lamin A(Davies et al., 2009; Shin & J.Worman, 2021). This incorrectly localized lamin A

causes alterations in the structure of the nuclear lamina and is sufficient to cause HGPS(Davies et al., 2009; Goldman et al., 2004). This connection between aberrant lamin A biogenesis and disease highlights the importance of correct cleavage and raises the possibility that this processing can be regulated.

O-GlcNAc Transferase is a potential regulator of lamin A processing (Simon et al., 2018). OGT is an enzyme that adds a single O-linked sugar (O-GlcNAc) at Ser and Thr residues on nuclear, mitochondrial, and cytoplasmic proteins (Bond & Hanover, 2015; Hart & Copeland, 2010; Levine & Walker, 2016). Lamin A is an OGT target (Simon et al., 2018), raising the possibility that this nuclear lamina protein is regulated by this post-translational modification. Specifically, an O-GlcNAc site is found in close proximity to the ZMPSTE24 cut site at T643 (Simon et al., 2018). Additionally, a previously identified OGT binding motif, DNLVTRS (Hrit et al., 2018), is located immediately N-terminal to the cleavage site(Simon et al., 2018). The proximity of the OGT binding motif and O-GlcNAc modification sites to the cleavage point on the lamin A tail suggests that O-GlcNAc modifications and/or OGT interaction may regulate lamin A processing.

We set out to test whether O-GlcNAcylation regulates lamin A processing using cells with natural variation in OGT levels, pharmacological inhibition of OGT, and an overexpression system to measure tail cleavage efficiency. Our results suggest that O-GlcNAcylation promotes lamin A processing. Exploring OGT as a novel regulator of this processing will provide insight into one molecular mechanism driving proper nuclear lamina assembly, which may be relevant to laminopathies.

Methods

Cell Culture Conditions

LF2 and E14 mESCs were routinely passaged in serum + LIF mESC media (500 mL KO-DMEM, 10% FBS, 2 mM L-glutamine, 1X non-essential amino acids, 0.1 mM 2-mercaptoethanol and recombinant leukemia inhibitory factor) on gelatin coated tissue-culture dishes. HEK293T cells were maintained in DMEM supplemented with 10% FBS and 1X PenStrep. OSMI-4 (Sellek) or Thiamet G (Medchem Express) was added 24 hours post passage, and cells were harvested 4 hours or 48 hours later. To induce lamin A constructs, 1 µg/mL Doxycycline was added for 24 hours.

Immunostaining

Trypsinized mESCs were cytospun onto octospot slides at 800 rpm for 3 minutes then fixed in 4% PFA for 10 minutes and washed with PBST. Fixed cells were permeablized in PBS + 0.01% TritonX-100 for 10m at room temperature and rinsed in PBST. Slides were then incubated in IF blocking buffer (10% Goat Serum, 100 µL fish skin gelatin, PBST) for 1 hour at room temperature. Slides were incubated in primary antibodies (*Supplementary Methods Table 1)* for 1 hour at room temperature and then washed 3 times in PBST. Slides incubated in fluorescent conjugated secondary antibody (*Supplementary Methods Table 2)* for 1 hour at room temperature in the dark. Slides were again washed 3 times in PBST, with the addition of DAPI in the second wash. Probed slides were mounted with prolong gold and stored at 4ºC. All primary and secondary antibodies used are listed in Methods Table 1 and Table 2.

Image Acquisition and Analysis

Fixed and immunostained slides were imaged on a Nikon Ti inverted fluorescence microscope with CSU-22 spinning disk confocal and a 60x, 1.4 numerical aperture, oil objective. 16-bit ND2 images were acquired in 0.3 µm step Z-stacks using an EMCCD camera. Specific Z-slices were chosen and cropped for figures in FIJI. Nuclear intensity analysis was performed in CellProfiler. CellProfiler outputs were processed in r and graphed with Prism. P-values calculated with unpaired t-test in Prism.

Nuclei Isolation

Cells were harvested, washed in PBS, and resuspended in Nuclei Preparation buffer I (320 mM sucrose, 10 mM Tris (pH 8.0), 3 mM $CaCl_2$, 2 mM $Mg(OAc)_2$, 0.1 mM EDTA, 0.1% Triton X-100, 1X protease inhibitors, and 1X phosphatase inhibitors) and dounce-homogenized on ice until >95% of nuclei stained by Trypan blue. Two volumes of nuclear preparation buffer II (2.0 M sucrose, Tris (pH 8.0), 5 mM $Mg(OAc)_2$, 5 mM DTT, 20 µM Thiamet G, 1X protease inhibitors, and 1X phosphatase inhibitors) were added to the nuclei suspension. Nuclei were pelleted by ultracentrifugation at 130,000 × g at 4°C for 45 min. Pelleted nuclei were washed with cold PBS and stored at −80°C.

Immunoblotting

Cells were released from tissue-culture dish and washed 1X in PBST. For endogenous lamin A blots, cell pellets were resuspended in urea lysis buffer (8 M Urea, 75 mM NaCl, 50 mM Tris pH 8.0, 1X Complete protease inhibitor tablet, and 1X phosphatase

Inhibitor) and sonicated using a probe sonicator in 10s on/30s off cycle for 3 cycles at 30% amplitude on ice. Total protein was quantified with Pierce BCA Assay Kit (Fisher). Urea lysates were run on a BioRad 4-20% MiniProtean-TGX gel and transferred to PVDF (0.2 µm, BioRad). Blots were then blocked in 5% milk and incubated in primary antibody (*Supplementary Methods Table 1*) at 4 ºC overnight. Blots were incubated with HRP-Conjugated secondary antibody (*Supplementary Methods Table 2*) and visualized with Pierce™ ECL Western Blotting Substrate.

For lamin A tail blots, 293T pellets were lysed in RIPA (150mM sodium chloride, 1% NP-40, 0.5% sodium deoxycholate, 0.1% sodium dodecyl sulfate, 50mM Tris, pH 8.0, 20 µM Thiamet-G, 1X protease inhibitors, 1X phosphatase inhibitors) for 20m while rotating at 4 ºC. Total protein was quantified with Pierce BCA Assay Kit (Fisher). Lysates were run on a hand-poured 12% acrylamide gel and transferred to PVDF. Blots were then blocked in 5% milk (Carnation) and incubated in primary antibody (*Table S1*) at 4 ºC overnight. Blots were incubated with fluorescently conjugated secondaries (*Table* S2) and visualized with LiCor imaging system. Band intensity was quantified in ImageStuido, further analyzed with r, and graphed with Prism. P-values calculated with one-way Anova test.

Sample Preparation for TMT

Nuclei preparations were lysed in TMT-optimized buffer (8M urea, 75 mM NaCl, 50 mM HEPES pH 8, 20µM Thiamet-G, 1X protease inhibitors, and 1X phosphatase inhibitors) and sonicated in 10s on/30s off cycle for 3 cycles at 30% amplitude. Total protein was

quantified with Pierce BCA Assay Kit (Fisher). 200μg total protein was set aside for mass spectrometry. Samples were diluted to 1 mg/mL in 5% SDS, 100 mM TEAB, and 25 μg of protein from each sample was reduced with dithiothreitol to 2 mM, followed by incubation at 55°C for 60 minutes. Iodoacetamide was added to 10 mM and incubated in the dark at room temperature for 30 minutes to alkylate the proteins. Phosphoric acid was added to 1.2%, followed by six volumes of 90% methanol, 100 mM TEAB. The resulting solution was added to S-Trap micros (Protifi), and centrifuged at 4,000 x g for 1 minute. The S-Traps containing trapped protein were washed twice by centrifuging through 90% methanol, 100 mM TEAB. 1 μg of trypsin was brought up in 20 μL of 100 mM TEAB and added to the S-Trap, followed by an additional 20 μL of TEAB to ensure the sample did not dry out. The cap to the S-Trap was loosely screwed on but not tightened to ensure the solution was not pushed out of the S-Trap during digestion. Samples were placed in a humidity chamber at 37°C overnight. The next morning, the S-Trap was centrifuged at 4,000 x g for 1 minute to collect the digested peptides. Sequential additions of 0.1% TFA in acetonitrile and 0.1% TFA in 50% acetonitrile were added to the S-trap, centrifuged, and pooled. Samples were frozen and dried down in a Speed Vac (Labconco) prior to TMTpro labeling.

TMT Labeling

Samples were reconstituted in TEAB to 1 mg/mL, then labeled with TMTpro 16plex reagents (Thermo Fisher) following the manufacturers protocol. Briefly, TMTpro tags were removed from the -20°C freezer and allowed to come to room temperature, after which acetonitrile was added. Individual TMT tags were added to respective samples,

and the reaction was allowed to occur at room temperature for 1 hour. 5% hydroxylamine was added to quench the reaction, after which the samples for each experiment were combined into a single tube. Since we performed quantitation on the unlabeled peptides, 0 day samples were added to four of the unused channels, increasing the signal for the unlabeled peptides. TMTpro tagged samples were frozen, dried down in the Speed Vac, and then desalted using homemade C18 spin columns to remove excess tag prior to high pH fractionation.

High pH Fractionation for TMT

Homemade C18 spin columns were activated with two 50 μL washes of acetonitrile via centrifugation, followed by equilibration with two 50 μL washes of 0.1% TFA. Desalted, TMTpro tagged peptides were brought up in 50 μL of 0.1% TFA and added to the spin column. After centrifugation, the column was washed once with water, then once with 10 mM ammonium hydroxide. Fractions were eluted off the column with centrifugation by stepwise addition of 10 mM ammonium hydroxide with the following concentrations of acetonitrile: 2%, 3.5%, 5%, 6.5%, 8%, 9.5%, 11%, 12.5%, 14%, 15.5%, 17%, 18.5%, 20%, 21.5%, 27%, and 50%. The sixteen fractions were concatenated down to 8 by combining fractions 1 and 9, 2 and 10, 3 and 11, etc. Fractionated samples were frozen, dried down in the Speed Vac, and brought up in 0.1% TFA prior to mass spectrometry analysis.

Mass Spectrometry for TMT

Peptides from each fraction were injected onto a homemade 30 cm C18 column with 1.8 um beads (Sepax), with an Easy nLC-1200 HPLC (Thermo Fisher), connected to a Fusion Lumos Tribrid mass spectrometer (Thermo Fisher). Solvent A was 0.1% formic acid in water, while solvent B was 0.1% formic acid in 80% acetonitrile. Ions were introduced to the mass spectrometer using a Nanospray Flex source operating at 2 kV. The gradient began at 3% B and held for 2 minutes, increased to 10% B over 7 minutes, increased to 38% B over 94 minutes, then ramped up to 90% B in 5 minutes and was held for 3 minutes, before returning to starting conditions in 2 minutes and re-equilibrating for 7 minutes, for a total run time of 120 minutes. The Fusion Lumos was operated in data-dependent mode, with both MS1 and MS2 scans acquired in the Orbitrap. The cycle time was set to 3 seconds. Monoisotopic Precursor Selection (MIPS) was set to Peptide. The full scan was done over a range of 400-1500 m/z, with a resolution of 120,000 at m/z of 200, an AGC target of 4e5, and a maximum injection time of 50 ms. Peptides with a charge state between 2-5 were picked for fragmentation. Precursor ions were fragmented by higher-energy collisional dissociation (HCD) using a collision energy of 38% and an isolation width of 1.0 m/z. MS2 scans were collected with a resolution of 50,000, a maximum injection time of 105 ms, and an AGC setting of 1e5. Dynamic exclusion was set to 45 seconds.

Data Analysis for TMT

Raw data was searched using the SEQUEST search engine within the Proteome Discoverer software platform, version 2.4 (Thermo Fisher), using the Uniprot mouse

database (downloaded January 2020). Trypsin was selected as the enzyme allowing up to 2 missed cleavages, with an MS1 mass tolerance of 10 ppm, and an MS2 mass tolerance of 0.025 Da. Carbamidomethyl on cysteine, and TMTpro on lysine and peptide N-terminus were set as a fixed modification, while oxidation of methionine was set as a variable modification. Percolator was used as the FDR calculator, filtering out peptides which had a q-value greater than 0.01. Reporter ions were quantified using the Reporter Ions Quantifier node, with an integration tolerance of 20 ppm, and the integration method being set to "most confident centroid". Protein abundances were calculated by summing the signal to noise of the reporter ions from each identified peptide, while excluding any peptides with an isolation interference of greater than 40%, or SPS matches less than 65%. Further calculations were done in R and graphed in Prism.

Sample Preparation for SILAC

XX and XY mESCs were grown under standard conditions using DMEM for SILAC, 10% dialyzed FBS, 2mM glutamine, 1X non-essential amino acids, 0.1mM b-mercaptoethanol, and recombinant leukemia inhibitory factor. XX mESCs were grown in light isotopes, L-Arginine HCl and L-Lysine-HCl. XY mESCs were grown in heavy isotopes, L-Lysine-2HCl (13C6, 15N2) and L-Arginine-HCl (13C6, 15N4) supplemented with 200 mM proline to avoid arginine-to-proline conversion. Cells were trypsinized, washed twice with cold PBS and then sonicated in 67 mM ammonium bicarbonate containing 8M guanidine HCl, 8X Phosphatase Inhibitor Cocktails II and III (Sigma-Aldrich), and 80 uM PUGNAc (Tocris Bioscience). Protein concentrations were

estimated with bicinchoninic acid protein assay (ThermoFisher Scientific). 10 mg of each lysate were combined, reduced for 1 h at 56°C with 2.55 mM TCEP and subsequently alkylated using 5 mM iodoacetamide for 45 min at room temperature in the dark. Lysates were diluted to 1M guanidine HCl using 50 mM ammonium bicarbonate, pH 8.0, and digested overnight at 37°C with sequencing grade trypsin (ThermoFisher Scientific) at an enzyme to substrate ratio of 1:50 (w/w). Tryptic peptides were acidified with formic acid (Sigma-Aldrich), desalted using a 35 cc C18 Sep-Pak SPE cartridge (Waters), and dried to completeness using a SpeedVac concentrator (Thermo).

Lectin Weak Affinity Chromatography for SILAC

Glycopeptides were enriched as described previously(Maynard & Chalkley, 2021; Trinidad et al., 2012) . Briefly, desalted tryptic peptides were resuspended in 1000 μl LWAC buffer (100 mM Tris pH 7.5, 150 mM NaCl, 2 mM $MgCl_2$, 2 mM $CaCl_2$, 5% acetonitrile) and 100 μl was run over a 2.0 x 250-mm POROS-WGA column at 100 μl/min under isocratic conditions with LWAC buffer and eluted with a 100-μl injection of 40 mM GlcNAc. Glycopeptides were collected inline on a C18 column (Phenomenex). Enriched glycopeptides from 10 initial rounds of LWAC were eluted with 50% acetonitrile, 0.1% FA in a single 500-μl fraction, dried. LWAC enrichment was repeated for a total of three steps.

Offline Fractionation for SILAC

Glycopeptides were separated on a 1.0 × 100 mm Gemini 3µ C18 column (Phenomenex). Peptides were loaded onto the column in 20 mM NH_4OCH_3, pH 10 and subjected to a gradient from 1 to 21% 20 mM NH_4OCH_3, pH10 in 50% acetonitrile over 1.1 mL, up to 62% 20 mM NH_4OCH_3, pH10 in 50% acetonitrile over 5.4 mL with a flow rate of 80 µL/min.

SILAC Mass Spectrometry Analysis

Glycopeptides were analyzed on an Orbitrap Fusion Lumos (Thermo Scientific) equipped with a NanoAcquity UPLC (Waters). Peptides were fractionated on a 15 cm × 75 µM ID 3 µM C18 EASY-Spray column using a linear gradient from 2% to 30% solvent B over 65 min. Precursor ions were measured from 350 to 1800 m/z in the Orbitrap analyzer (resolution: 120,000; AGC: 4.0e5). Each precursor ion (charged 2–8+) was isolated in the quadrupole (selection window: 1.6 m/z; dynamic exclusion window: 30 s; MIPS Peptide filter enabled) and underwent EThcD fragmentation (Maximum Injection Time: 250 ms, Supplemental Activation Collision Energy: 25%) measured in the Orbitrap (resolution: 30,000; AGC; 5.04). The scan cycle was 3 s. Peak lists for EThcD were extracted using Proteome Discoverer 2.2. EThcD peak lists were filtered with MS-Filter, and only spectra containing a 204.0867 m/z peak corresponding to the HexNAc oxonium ion were used for database searching. EThcD data were searched against mouse and bovine entries in the SwissProt protein database downloaded on Sept 06, 2016, concatenated with a randomized sequence for each entry (a total of 22,811 sequences searched) using Protein Prospector (v5.21.1). Cleavage specificity

was set as tryptic, allowing for two missed cleavages. Carbamidomethylation of Cys

was set as a constant modification. The required mass accuracy was 10 ppm for

precursor ions and 30 ppm for fragment ions. Variable modifications are listed in

Supplemental Methods Table 3. Unambiguous PTMs were

determined using a minimum SLIP score of six, which corresponds to a 5% local false

localization rate(Baker et al., 2011) . Modified peptides were identified with a peptide

false discovery rate of 1%. O-GlcNAc and O-GalNAc modifications were differentiated

based on known protein subcellular localization and HexNAc oxonium ion fragments

138/144 ratio(Halim et al., 2014; Maynard & Chalkley, 2021) . Comparison with TMT

dataset was done in R and graphed in Prism.

Generation of Inducible lamin A Tail Lines

Lamin A Tail constructs were created in an XLone-GFP plasmid (Randolph et al.,

2017) by inserting a custom gBlock (IDT, *Supplementary Figure S3*) containing an NLS

and the 44-amino acid lamin A tail into XLone-GFP with the NEB HiFi Assembly Kit.

Next, point mutations were made using the NEB Site-Directed Mutagenesis Kit for

primer design (*Supplementary Table S4*) and assembly. Lamin A tail plasmids were co-

transfected with PiggyBac Transposase(Randolph et al., 2017) with Lipofectamine 2000

(Fisher). Transfections incubated for 48 hours, and transfection media was replaced

with Blasticidin selection media (DMEM, 10% FBS, 1X Pen/Strep, 6 μM Blasticidin).

After selection, cells were induced with 1 μM doxycycline for 24 hours and then sorted

for GFP expression (BD FACS Aria Fusion).

Results

OGT and O-GlcNAc marks are more abundant in XX mESC nuclei

O-GlcNAcylation of lamin A suggests OGT as a potential regulator of lamin A processing(Simon et al., 2018). We sought to explore cell types in which there is natural variation in OGT abundance to assess how OGT may regulate lamin A. We used mouse embryonic stem cells because female mESCs have two active X chromosomes while male (XY) mESCs have one active X chromosome. As OGT is X-linked, XX mESCs express higher levels of OGT than males (E. A. Martin et al., 2021). Thus, these two cell lines, that otherwise have the same developmental potential, differ in OGT abundance and provide a model system to study the effects of OGT levels on the nuclear lamina. First, we assessed OGT distribution and abundance in male and female mESCs via immunostaining and showed that OGT is concentrated in the nucleus of XX mESCs while it accumulates in the cytoplasm of XY mESCs (Figure 1A), as was previously shown(E. A. Martin et al., 2021). The nuclear intensity of OGT was quantified, showing that XX mESCs have more nuclear OGT than XY mESCs (Figure 1B). Additionally, immunoblotting of nuclear and whole cell extracts show a greater abundance of OGT in XX mESC nuclei than in XY mESC nuclei (Figure 1C and 1D). These results establish that there is a difference in OGT abundance between XX and XY mESC nuclei, making them a useful system to study the effects of variation in OGT levels on the nuclear lamina.
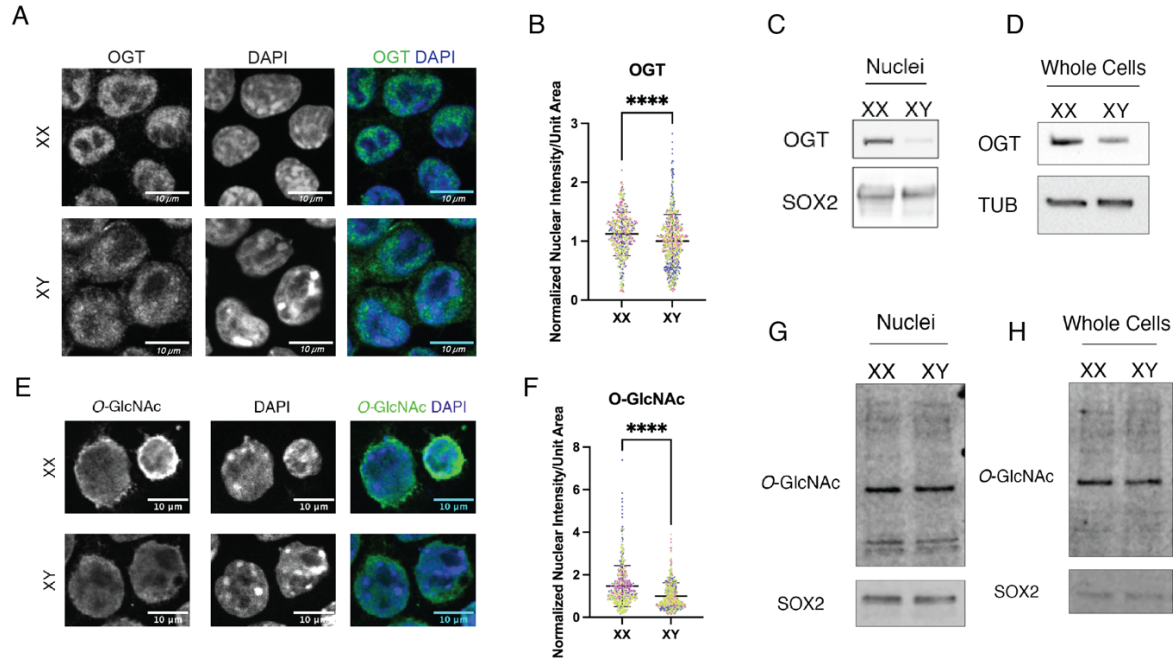
Figure 2.1 *Nuclear OGT correlates with high levels of O-GlcNAcylation in XX mESCs*
A) Confocal imaging of immunofluorescence staining of OGT on XX and XY mESCs.
Representative middle slices were chosen. Scale bar is 10µm. (B) Quantitation of
nuclear fluorescence intensity per unit area of OGT signal represented in (A) Data
represents quantitation of 3 independent experiments with individual replicates indicated
by distinct colors. Each experiment was normalized by the mean value of XY cells. (C)
OGT immunoblot of XX and XY mESC nuclear extracts. 20µg nuclear protein loaded
per lane. SOX2 represents loading control. (D) OGT immunoblot of XX and XY mESCs.
20µg whole cell lysate loaded per lane. TUB represents loading control (E) Confocal
imaging of immunofluorescence staining of *O*-GlcNAcylation on XX and XY mESCs.
Representative middle slices were chosen. Scale bar is 10µm. (F) Quantitation of
nuclear fluorescence intensity per unit area of *O*-GlcNAc signal represented in (E). Data
represents quantitation of 3 independent experiments with individual replicates indicated
by distinct colors. Each experiment was normalized by the mean value of XY cells. (G)
O-GlcNAc immunoblot of XX and XY mESC nuclear extracts. 20µg nuclear extract
loaded per lane. SOX2 represents loading control for stem cell nuclei. (H) *O*-GlcNAc
immunoblot of XX and XY mESCs. 20µg whole cell protein loaded per lane. SOX2
represents loading control for stem cell nuclei. **** p < 0.0001

O-GlcNAc enriched proteomics reveals highly O-GlcNAc modified nuclear proteins

Higher levels of OGT in the XX mESC nuclei correlate with increased nuclear *O*-GlcNAc immunostaining (Figure 1 E and 1F). However, a difference in total abundance of *O*-GlcNAc in nuclei and whole cells was not detectable by immunoblotting (Figure 1G and 1H). To more sensitively query effects of the nuclear accumulation of OGT on protein abundance and *O*-GlcNAc modification in XX mESCs, we used unbiased multiplexed proteomics approaches.

First, we sought to correlate the number of active X chromosomes with nuclear protein abundance. To make this comparison, we employed tandem mass tagging (TMT) coupled with LC-MS/MS using XX, XY, and XO cells (which are XX cells that have lost one X chromosome). In two separate experiments, we compared XX mESC nuclei with XY or XO mESC nuclei and calculated the Log2 fold-change of identified proteins. The Log2 fold-change values were then graphed in a correlation plot with the XX/XO value on the Y-axis and the XX/XY value on the X-axis. The correlation plots show that most proteins do not correlate with the number of X chromosomes (Figure 2A). The most prominent downregulated proteins are all autosomal, and some, like DNMT3a, are known to be more highly expressed in XY mESCs(Schulz et al., 2014; Zvetkova et al., 2005). In contrast, OGT positively correlates with the number of Xs, as it is X-linked and more abundant in the XX mESC nuclei in both the XY and XO comparisons. Other highly enriched proteins in the XX cells include HMGB3, PGRC1, and EMD, all of which are X-linked and thus expected to be more abundant in the XX mESCs. The most highly abundant autosomal protein in the XX cells compared to both

XY and XO cells is lamin A/C, suggesting that lamin A/C abundance is correlated to the number of Xs.

Next, we were interested in determining which abundant proteins in the XX mESCs are also *O*-GlcNAc modified. We performed *O*-GlcNAc enriched stable isotope labeling using amino acids in cell culture (SILAC) mass spectrometry by growing XX and XY cell populations in heavy and light media. Labeled cells were pooled and lysed, and tryptic digests were run on a lectin weak affinity chromatography column to enrich for *O*-GlcNAcylated peptides which were quantified by EThcD-MS/MS (Figure 2B). In comparing the proteins enriched in XX nuclei from the TMT dataset to the identified *O*-GlcNAc modified peptides, we found X-linked OGT targets, such as emerin. In addition, some autosomal proteins that have an OGT interaction motif were highly *O*-GlcNAc modified, including TET1 and lamin A (Figure 2C). Some nuclear proteins that are highly *O*-GlcNAc modified, including nucleoporins (Bond & Hanover, 2015), do not exhibit increased *O*-GlcNAcylation in XX relative to XY mESC nuclei, suggesting that lamin A and TET1 are specifically X chromosome dose dependent. Analysis of individual lamin A peptides revealed two putative *O*-GlcNAc sites in the tail at S613 and T643 (Figure 2D, 2E). Our identification of these two sites supports previous work mapping *O*-GlcNAc marks at the same locations in liver cells (Simon et al., 2018).
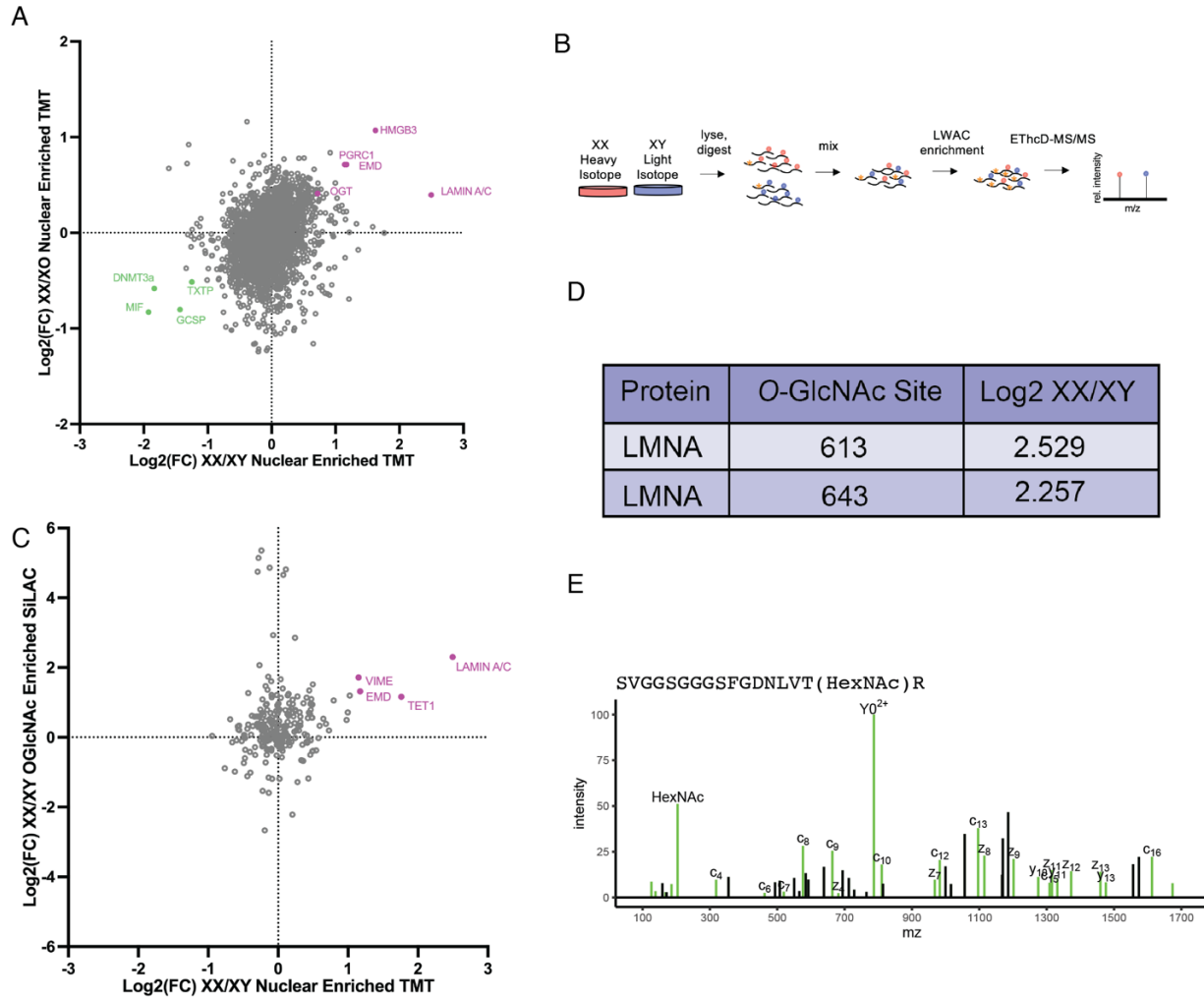
Figure 2.2 *Quantitative proteomics identifies nuclear proteins that are highly O-GlcNAc modified in XX mESCs.* (A) TMT results graphed as correlation plot of log2 fold-change of protein abundance in XX vs XY nuclei (x-axis) and XX vs XO nuclei (y-axis). (B) XX and XY mESCs were grown in heavy and light isotope media, respectively, and combined. Tryptic digests of combined samples were subject to lectin weak affinity chromatography (LWAC) to enrich for *O*-GlcNAcylated peptides. EThcD-MS/MS identified peptides and *O*-GlcNAc sites. (C) Correlation plot of log2 fold-change of protein abundance in XX vs XY nuclei (x-axis) and proteins with *O*-GlcNAc enriched peptides in XX vs XY whole cells (y-axis). (D) Table of *O*-GlcNAcylated peptides in lamin A and their fold change (XX/XY). (E) Spectrum of lamin A peptide that contains *O*-GlcNAcylation at T643.

Lamin A is highly expressed in XX mEScs

XY mESCs express low levels of lamin A(Burke & Stewart, 2013; Eckersley-Maslin et al., 2013), prompting us to query the distribution of lamin A in XX mESCs. Immunofluorescence staining in XX and XY mESCs shows that lamin A is more abundant at the nuclear periphery in XX mESCs compared to the XY mESCs (Figure 3A and B). Immunoblot of nuclear extracts also show that both lamin A and lamin C are not detectable in XY mESC nuclei, while they are detectable in XX mESCs (Figure 3C). The positive correlation between the number of X-chromosomes and the amount of *O*-GlcNAcylated lamin A suggests that OGT dose may underlie lamin A abundance in XX mESCs.
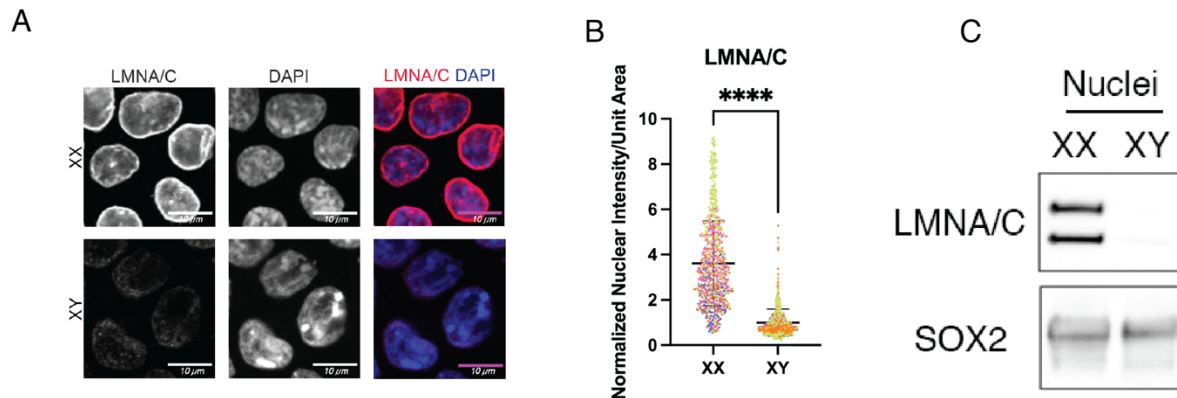
Figure 2.3 *Lamin A is abundant in XX mESCs.* (A) Confocal imaging of immunofluorescence staining of lamin A/C on XX and XY mESCs. Scale bar is 10μm. (B) Quantitation of nuclear fluorescence intensity per unit area of lamin A/C signal represented in (A). Data represents quantitation of 4 independent experiments with individual replicates indicated by distinct colors. Each experiment was normalized by the mean value of XY cells. (C) Lamin A/C immunoblot of XX and XY mESC nuclear extracts. 20μg nuclear protein loaded per lane. SOX2 represents loading control for stem cell nuclei. **** $p < 0.0001$

Cellular O-GlcNAc levels do not affect lamin A protein abundance or distribution

To further understand the potential regulatory relationship between lamin A and OGT, we wanted to perturb the dosage of OGT in the XX mESCs. *OGT,* however, is an essential gene and deletion of just one copy of *OGT* is embryonic lethal in mice (Shafi et al., 2000). To circumvent the challenges of genetic manipulations, we utilized a chemical OGT inhibitor, OSMI-4 (S. E. S. Martin et al., 2018). OSMI-4 is a competitive inhibitor of OGT, that binds the active site. Treatment with OSMI-4 results in a successful decrease in overall *O*-GlcNAcylation in XX mESCs (Figure 4A and D). OGT abundance, however, increases with OSMI-4 treatment (Figure 4A and C). OGT homeostasis is tightly regulated, and this high OGT abundance is likely due to a feedback loop that increases OGT expression when its function or expression is perturbed (Stephen et al., 2021). The overall decrease in *O*-GlcNAcylation due to OSMI-4 treatment did not cause a significant decrease in lamin A/C abundance or distribution (Figure 4B and E). Lamin A/C does co-localize with lamin B1, suggesting correct localization at the nuclear lamina (Figure S1). Whole cell immunoblots additionally show the change in abundance of OGT and *O*-GlcNAcylation but not lamin A (Figure 4F). These results suggest that the overall abundance of mature lamin A is not impacted by decreased OGT activity.
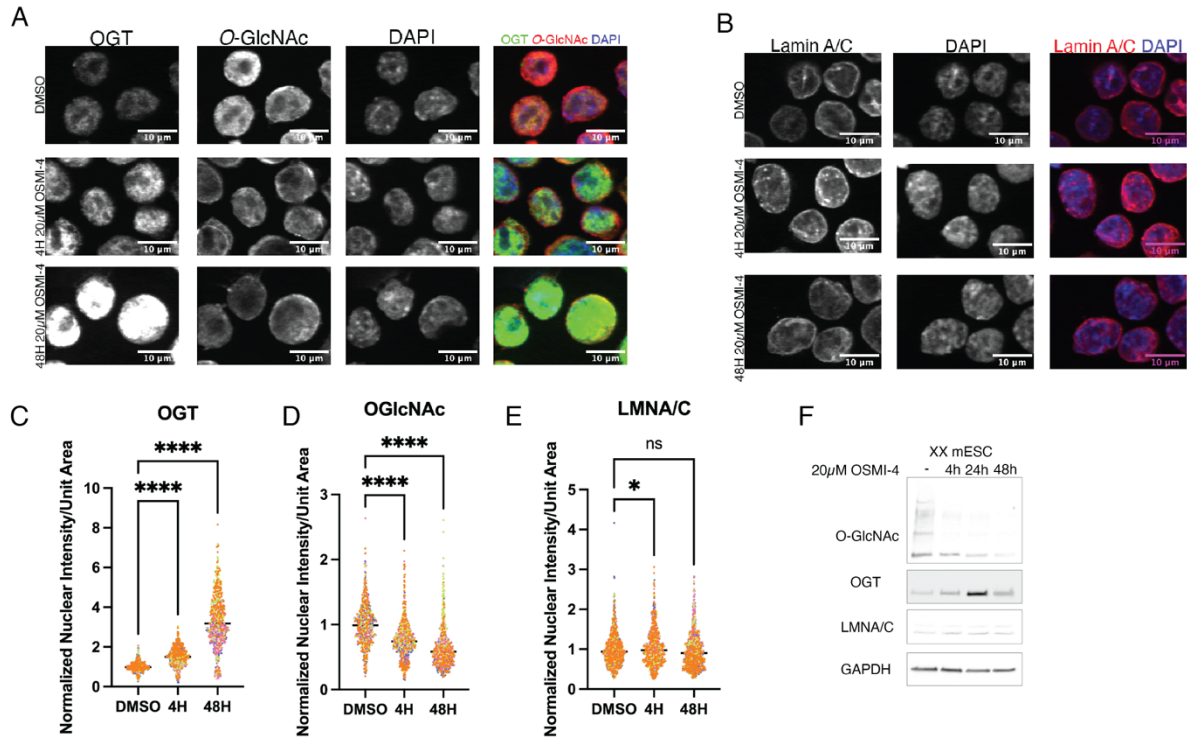
Figure 2.4 *Perturbation of OGT activity in mESCs does not affect LMNA abundance or distribution.*(A) Confocal imaging of immunofluorescence staining of OGT and O-GlcNAc on XX mESCs treated with 20µM OSMI-4 for 4 or 48 hours or with DMSO for 48 hours. Scale bar is 10µm. (B) Confocal imaging of immunofluorescence staining of lamin A/C on XX mESCs treated with 20µM OSMI-4 for 4 or 48 hours or with DMSO for 48 hours. Scale bar is 10µm. (C)-(E) Quantitation of nuclear fluorescence intensity per unit area of OGT (C) and *O*-GlcNAc (D) signal represented in (A), and lamin A (E) signal represented in (B). Data represents quantitation of 4 independent experiments with individual replicates indicated by distinct colors. Each experiment was normalized to the mean of the DMSO control. (F) Immunoblot of whole cell extracts for *O*-GlcNAc, OGT, and lamin A/C after treatment with 20µM OSMI-4 or DMSO for 4, 24, and 48 hours. GAPDH represents loading control.
 * $p < 0.05$ **** $p < 0.0001$ ns = not significant

OGT promotes lamin A tail cleavage

Treatment with OSMI-4 both caused an increase in OGT abundance and a

decrease in *O*-GlcNAcylation which complicates interpretation. The location of the OGT

binding and *O*-GlcNAc modification sites suggests that OGT may regulate lamin A

cleavage. Therefore, we directly assayed the contributions of the OGT binding motif and the *O*-GlcNAcylation sites in a lamin A tail cleavage assay (Barrowman et al., 2012; Spear et al., 2019). The T643 modification site is located just N-terminal to the ZMPSTE24 cleavage site in lamin A (Burke & Stewart, 2013; Davies et al., 2009). In the same region, there is also a previously identified OGT binding motif (Hrit et al., 2018) (Figure 5A). Doxycycline-inducible overexpression constructs encoding GFP-NLS-lamin A tails carrying point mutations that perturb *O*-GlcNAc sites and/or the OGT interaction motif (Figure 5B) were integrated into HEK 293T cells. Tail constructs primarily localize to the nucleus, but do not accumulate at the nuclear periphery (Figure S2). Roughly 24-hours after induction quantitative immunoblots were performed to resolve cleaved and uncleaved lamin A tail species (Figure 5C), and cleavage efficiency was quantified as the proportion of cleaved lamin A tail versus the total lamin A tail expression (cleaved + uncleaved). The cleavage efficiency was then normalized to WT, such that the WT cleavage efficiency is set at 1.0. Cleavage efficiency decreased with mutation of the Asp 639 to Ala (D639A), a mutation that disrupts the OGT binding motif (Hrit et al., 2018). Because mutation of one *O*-GlcNAcylated residue can result in modification of nearby Ser and Thr residues (Hart et al., 2007), we mutated both T643 and S645 alone and in combination. The double mutant of T643A and S645A has a significantly lower cleavage efficiency compared to each single mutant. The triple mutant (D639A, T643A, and S645A) showed the largest decrease in cleavage efficiency with an average of 48% of the lamin A tail construct properly cleaved (Figure 5D and E). It was previously reported that the D639A, T643A, and S645A mutations have negligible effects on lamin A tail cleavage efficiency (Babatz et al., 2021). However, these experiments were done in a

"humanized" yeast system that expresses ZMPSTE24 but does not express OGT. In total, these experiments indicate that both the OGT binding motif and the *O*-GlcNAc modified amino acids play a role in regulating the cleavage efficiency of the lamin A tail.

Overall cellular O-GlcNAc levels affects lamin A cleavage efficiency

While our mutagenesis experiments revealed the importance of specific amino acids to lamin tail cleavage efficiency, these experiments cannot distinguish between the effects of the amino acid substitution and post-translational modification. To query the extent to which lamin A tail cleavage may be regulated by *O*-GlcNAc, we performed the cleavage assays with the addition of the OSMI-4 inhibitor. Treatment with OSMI-4 for 48hrs decreased both overall *O*-GlcNacylation and the cleavage efficiency of the lamin A tail constructs; OSMI-4 treated cells had a normalized cleavage efficiency of 70% (Figure 5F and G). We also queried the effects of increasing O-GlcNAcylation by treating the cells with Thiamet-G (TMG), an inhibitor of *O*-GlcNAcase (OGA), the sole enzyme that removes *O*-GlcNAcylation (Bond & Hanover, 2015; Hart et al., 2007). TMG treatment increased overall *O*-GlcNacylation but did not affect overall cleavage efficiency (Figure 5H and I), suggesting that the WT cells cleave lamin A tails at a high rate that is not influenced by additional *O*-GlcNAcylation.

Next, we wanted to test the response of the cleavage assay in a system that shows more physiological relevance. Glucose is a necessary component for synthesis of UDP-GlcNAc, OGT's substrate, thus decreasing cellular glucose levels also decreases overall *O*-GlcNAcylation(Hart et al., 2007) To explore the relationship between glucose levels and lamin A cleavage efficiency, WT lamin A tail construct cell

lines were grown in 5 mM (low) glucose or 25 mM (high) glucose media. Cells grown in low glucose show a small but significant decrease in both overall *O*-GlcNAcylation and tail cleavage (Figure 5J and K). This small decrease in cleavage efficiency may be due to the partial effect of reducing glucose on *O*-GlcNAc abundance. Together with the OSMI-4 inhibitor results, our glucose manipulation results indicate that *O*-GlcNAcylation promotes tail cleavage. These results provide evidence of a new input into control of lamin A processing.
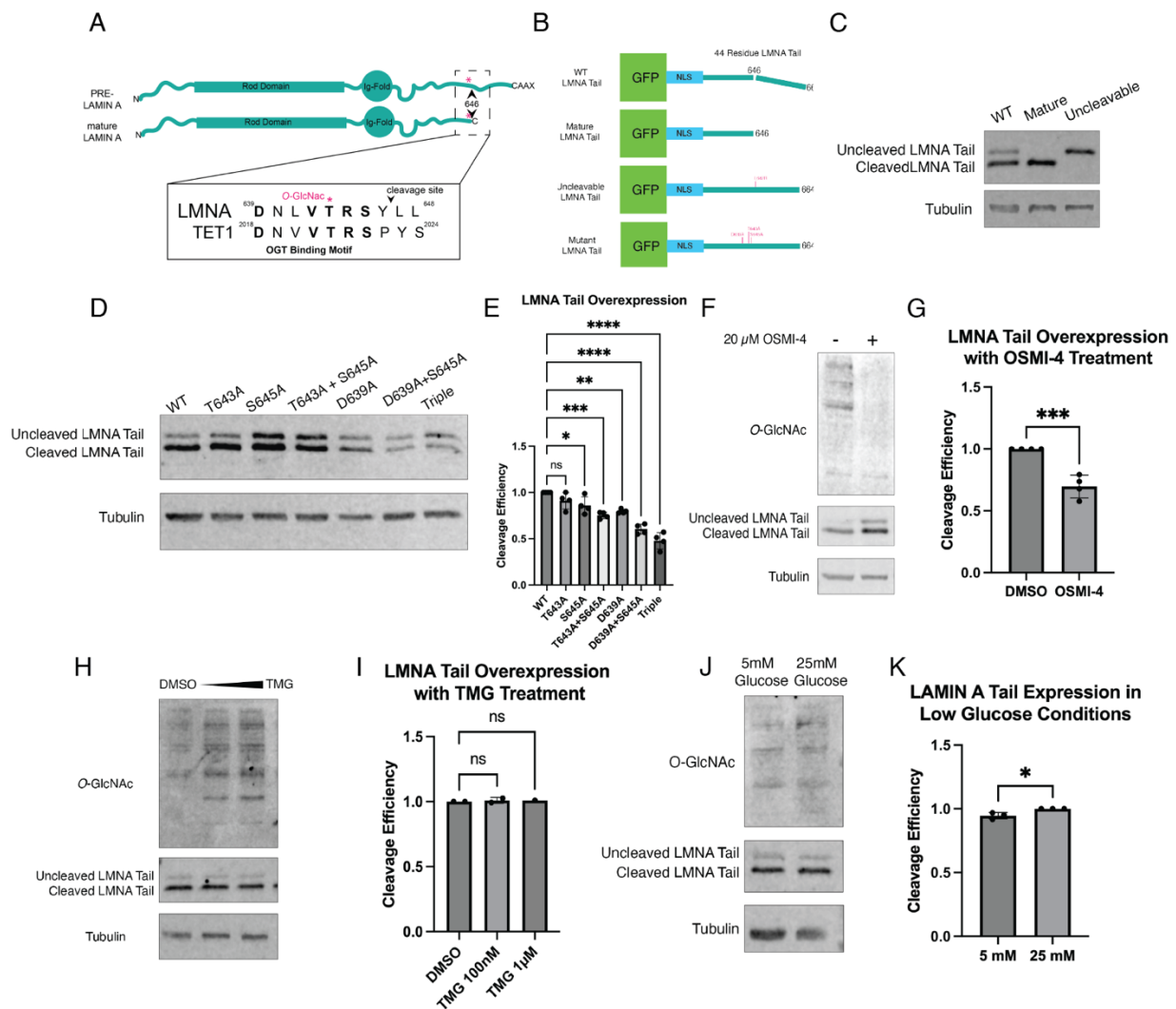

Figure 2.5 *O-GlcNAc modified residues promote lamin A tail processing*
(Figure legend continued on the next page)

(Figure legend continued from the previous page)
(A) Diagram of lamin A tail showing the location of the T643 *O*-GlcNAc site and the OGT binding motif. (B) Diagram of lamin A tail overexpression constructs and location of point mutations in relation to the cleavage site. (C) GFP immunoblot of control tail cleavage constructs demonstrating size difference of cleaved and uncleaved lamin A tail. Mature lamin A tail consists of a construct that ends at Y646, mimicking the C-terminus of mature lamin A. Uncleavable mutant contains L647R mutation that fully prevents cleavage of the lamin A tail. (D) Quantitative GFP immunoblot of lamin A tail point mutation constructs. Tail expression induced with 1μg/mL dox for approximately 24hrs. 20μg whole cell protein loaded per lane. (E) Quantitation of cleavage efficiency from (D). Band intensity is normalized to tubulin loading control and background subtraction calculated based on median background intensity above and below each band. Cleavage efficiency is calculated by dividing the intensity of the cleaved LMNA tail band over the total intensity of the cleaved and uncleaved LMNA tail bands and normalized to WT. Data represents quantitation of 3 independent experiments. (F) Quantitative immunoblot of WT lamin A tail treated with 20μM OSMI-4 or DMSO. (G) Quantitation of cleavage efficiency of OSMI-4 treated lamin A tails in (F) Data represents quantitation of 3 independent experiments. (H) Quantitative immunoblot of WT lamin A tail treated with 100nM and 1μM TMG or DMSO (I) Quantitation of cleavage efficiency of TMG treated lamin A tails in (H). Data represents quantitation of 3 independent experiments. (J) Quantitative immunoblot of WT lamin A tail grown in media with 5mM glucose and 25 mM Glucose for 48 hours. (K) Quantitation of cleavage efficiency of cells in low and high glucose media in (J). Data represents quantitation of 3 independent experiments.
* $p < 0.05$, ** $p < 0.01$, *** $p < 0.001$, **** $p < 0.0001$, ns = not significant

Discussion

Our results indicate that OGT may play a role in lamin A processing. Our data show that mutations to OGT binding and *O*-GlcNAc modification sites, OGT inhibition, and decreased glucose levels each reduce lamin A tail cleavage efficiency. However, perturbations to OGT dose do not appear to affect endogenous lamin A abundance and distribution.

In comparing lamin A abundance in XX vs XY mESCs, we have demonstrated that lamin A is more abundant in XX mESCs. In XY mESCs, lamin A expression ranges from undetectable to very low(Burke & Stewart, 2013; Eckersley-Maslin et al., 2013). In contrast, we find lamin A is easily detected in XX mESCs, suggesting a correlation

between X chromosome number and lamin A abundance. Lamin A is the non-X-linked protein that is most significantly enriched in XX nuclei in our quantitative proteomic data. However, in the XX vs XO dataset the relative enrichment of lamin A is lower, suggesting input from the Y chromosome may also play a role in lamin A expression. This difference in lamin A abundance highlights the importance of investigating sex difference at a cellular level as well as a whole organism level. Elucidating this relationship between sex chromosomes and lamin A may provide insight into the molecular mechanisms that control lamin A abundance.

In addition to finding more lamin A in XX mESCs, we also detected more *O*-GlcNAcylated lamin A, suggesting the overall increase in lamin A may underlie the increased abundance of the modified form. We identified two specific *O*-GlcNAc modification sites in the lamin A tail. The S613 modification is in a previously described "sweet spot"(Simon et al., 2018) among other Ser and Thr residues. The second *O*-GlcNAc site we identified, T643, is located just N-terminal to the ZMPSTE24 cleavage site at Y646. The proximity of T643 to the cleavage site suggests that this *O*-GlcNAc site may play a regulatory role in lamin A processing.

Additional highly *O*-GlcNAc modified proteins were detected in our mass spectrometry datasets. One such protein is emerin, which localizes to the nuclear periphery and interacts with lamin A(Koch & Holaska, 2014; Lee et al., 2001; Samson et al., 2018). Consistent with a prior report, we mapped *O*-GlcNAc sites in emerin in the unstructured, Ser-rich lamin A binding domain (Berk, Maitra, et al., 2013). As emerin is X-linked(Koch & Holaska, 2014), the high abundance of *O*-GlcNAcylation detected in

XX vs XY mESCs in the SILAC dataset may be the result of increased expression of emerin in the XX mESCs.

We tested whether the high levels of OGT in XX mESC nuclei were linked to the high levels of lamin A by pharmacologically inhibiting OGT. Treatment of XX mESCs with OSMI-4 did not affect lamin A abundance or localization at the nuclear periphery. In HGPS, misprocessing of lamin A leads to nuclei with drastic morphological defects, including nuclear blebbing, aggregated nuclear pores, as well as loss of peripheral heterochromatin (Eriksson et al., 2003; Goldman et al., 2004). However, we do not see these morphological changes when we inhibit OGT in the XX mESCs, suggesting that lamin A biogenesis is not detectably affected by this inhibition or that incorporation of incorrectly processed lamin A has no effect in XX mESCs. In some cell types, lamin A is a long-lived protein with slow turnover (Hasper et al., 2023). This long half-life in combination with our lack of tools to detect processing intermediates may complicate our ability to meaningfully query the effects of OGT inhibition on lamin A processing.

To more directly test lamin A processing, we examined the effects of mutation of OGT interaction and *O*-GlcNAcylation sites using an established tail cleavage assay(Barrowman et al., 2012; Spear et al., 2019). Introduction of mutations in the *O*-GlcNAc sites and/or the OGT binding motif in the lamin A tail reduced cleavage efficiency. In yeast, the same point mutants do not cause a large decrease in cleavage efficiency(Babatz et al., 2021). Yeast does not express OGT(Kreppel et al., 1997; Lubas et al., 1997), suggesting that the effects of mutations in human cells may in part be due to the presence of OGT. Consistent with the role of OGT, treatment with OSMI-4 also decreased the cleavage efficiency. Additionally, growth in low glucose media which

results in a decrease in abundance of the OGT co-factor UDP-GlcNAc and a concomitant decrease in *O*-GlcNAcylation(Hart et al., 2007), caused a slight but significant decrease in processing. The decreased cleavage efficiency due to mutations, OGT inhibition, and low cellular glucose suggests that while OGT binding and *O*-GlcNAc modifications are not necessary for lamin A tail cleavage, their presence on the tail enhances cleavage.

The mechanism behind this regulation remains to be understood. It is possible that the *O*-GlcNAc modifications stabilize the interaction between lamin A and its protease ZMPSTE24. Another possibility could be that the presence of OGT and the *O*-GlcNAc marks stabilized the lamin A tail in a conformation that promotes ZMPSTE24 cleavage. A major limitation to these experiments is the use of the tagged overexpression system to assess lamin A cleavage. While this overexpression system allows us to test many point mutations, we do not retain the larger biological context of the full-length protein. Perturbing *O*-GlcNAc sites or the OGT interaction domain on the endogenous protein in OGT expressing cells would provide more insight into the mechanism linking OGT to lamin A processing.

OGT acts as a link between the proteins it modifies and metabolic regulation, as glucose is a necessary component to synthesis of OGT's substrate UDP-GlcNAc(Hart et al., 2007). UDP-GlcNAc levels, and thus *O*-GlcNAcylation levels, are known to fluctuate in metabolic and neurodegenerative disease(Bond & Hanover, 2015; Hart et al., 2007). *O*-GlcNAc modification of lamin A could act as a metabolism linked regulator of lamin A processing, suggesting a model where the integrity of the nuclear lamina may be directly affected by these metabolic disorders. Lamin A processing efficiency is also

known to decrease with age(López-Otín et al., 2013). However, *O*-GlcNAcylation

increases with age(Fülöp et al., 2008; Lunde et al., 2012), perhaps in response to

decreased processing efficiency. Overall, this study provides evidence for the metabolic

regulation of the nuclear lamina, which may provide new insights into disease and

aging.

Chapter 3

OGT Homeostasis is Highly

Regulated

Introduction

Ogt is an essential gene that is highly regulated(Shafi et al., 2000). Previous work in mice has shown that even heterozygous *ogt* knockout in XX embryos is embryonic lethal(Shafi et al., 2000). Furthermore, the balance between OGT and OGA abundance is tightly regulated. Both OGT and OGA respond to feedback loops, thus when one enzyme is inhibited, the other is downregulated to recover *O*-GlcNAc homeostasis(Hart et al., 2007; Stephen et al., 2021; Tan et al., 2020).

One regulatory mechanism of both OGT and OGA is detained intron (DI) splicing. When OGT is inhibited and overall *O*-GlcNacylation decreases, the DI in *ogt* transcripts is lost and pushes homeostasis towards functional *ogt* mRNA(Tan et al., 2020). However, when OGA is inhibited and *O*-GlcNAcylation increases, the opposite occurs and the overall abundance of productive *ogt* transcripts decreases (Tan et al., 2020).

In this chapter, we tested the effects of genetic OGT dose manipulations in XX and XY mESCs by utilizing an inducible degron system to degrade protein from one copy of the *Ogt* in XX mESCs and overexpressing tagged *Ogt* in XY mESCs. We found that OGT dose is highly regulated in both cell types, causing changes in OGT expression to maintain *O*-GlcNAc homeostasis.

Methods

To induce the degradation of OGT protein in the FKBP-OGT XX mESC cell line, cells were treated with 0.5 μM dtag-13 (Tocris) for 48 hours and then harvested. All other experiments were performed according to the methods in Chapter 2.

Results

Degradation of OGT in XX mESCs

Ogt is an essential gene in mESCs, and heterozygous knockout of *Ogt* in mouse embryos is lethal (Shafi et al., 2000). To test the relationship between OGT dose and lamin A abundance, we utilized a cell line in which one allele of *Ogt* is tagged with an FKBP degron(Nabet et al., 2018). When the cells are treated with the small molecule dtag-13, it will binds the FKBP to an E3 ubiquitin ligase which will ubiquitinate the OGT and mark it for degradation by the proteasome(Nabet et al., 2018). Immunoblots of the induced OGT degron cell lines shows that the larger FKBP tagged OGT disappears when cells are treated with 0.5 μM dtag-13 for 48 hours compared to DMSO treatment (Figure 3.1A). However, the lower untagged OGT protein seems to increase in abundance when the OGT-FKBP is degraded. Additionally, degradation of OGT does not seem to affect lamin A abundance (Figure 3.1A).

Immunostaining shows variation in OGT and lamin A/C staining between WT XX mESCs and the OGT-FKBP cell line without dtag-13 treatment (Figure 3.1B-D). With OGT degradation, OGT and lamin A/C nuclear intensity increases, suggesting an increase in OGT expression from the second allele that compensates for the degradation of the FKBP-tagged OGT. Finally, to quantitatively assess the protein

abundance of OGT and lamin A after dtag-13 treatment, we performed TMT on WT,

DMSO treated OGT-FKBP cells, and dtag-13 treated FKBP-OGT cells. The TMT data

shows that the log2-fold changes of WT XX vs DMSO treated OGT-FKBP cells and

DMSO treated vs dtag-13 treated OGT-FKBP cells are close to zero (Figure 3.1E),

indicating no change in abundance of OGT and lamin A between the cell types. The

lack of change in OGT with the degron shows that the compensation of the untagged

allele reverts OGT dose back to that of WT XX mESCs, providing evidence to the highly

regulated nature of OGT homeostasis in mESCs.

Protein	Peptides	Log2 XX/DMSO	Log2 DMSO/Dtag
LMNA/C	35	0.083	-0.047
OGT	15	-0.003	-0.024
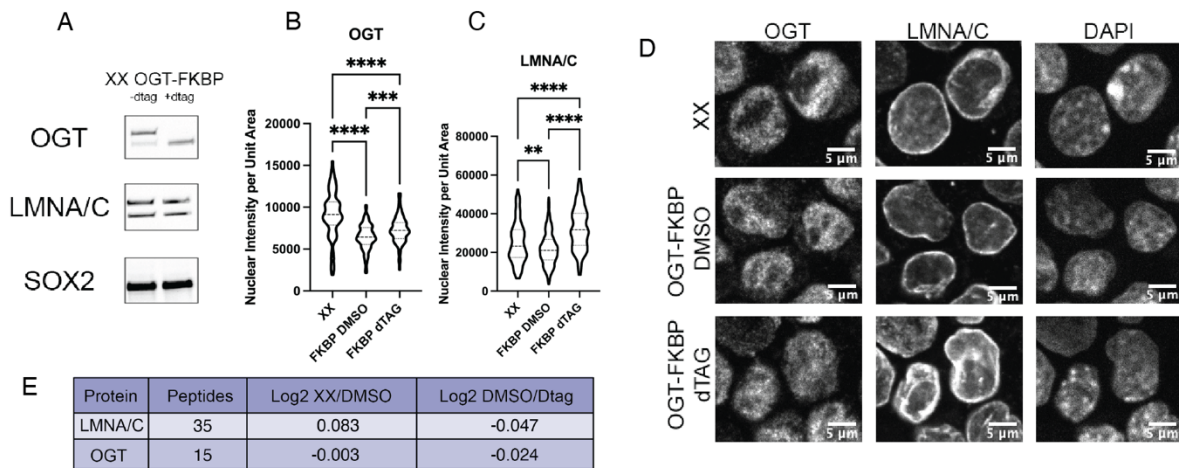
Figure 3.1 *OGT degradation causes upregulation of untagged allele*
(A) Immunoblot of OGT-FKBP XX mESC nuclei treated with either dTag or DMSO. OGT
staining shows upper (FKBP tagged) protein degrade with addition of dTag, but lower
band (untagged) increases in expression. (B) quantitation of nuclear intensity per unit
area of OGT immunofluorescent staining in (D). (C) quantitation of nuclear intensity per
unit area of lamin A/C immunofluorescent staining in (D). (D) Immunofluorescence of
OGT and lamin A/C with WT XX, XX OGT-FKBP treated with DMSO, and XX OGT-
FKBP treated with dTag. dTag treatment decreases OGT abundance slightly but does
not decrease lamin A/C abundance. (E) TMT quantitation of lamin A/C and OGT protein
in WT XX, XX OGT-FKBP treated with DMSO, and XX OGT-FKBP treated with dTag.
There does not seem to be any change in OGT or lamin A protein abundance with dTag
treatment. ** $p < 0.01$, *** $p < 0.001$, **** $p < 0.0001$

Overexpression of OGT in XY mESCs

　　To test perturbations to OGT dose in the opposite direction, we employed an XY

cell line that has an extra copy of OGT inserted randomly into the genome.

Immunofluorescence staining shows that these overexpressed (OE) OGT cells express

only slightly more OGT than WT XY cells (Figure 3.2A and B). Lamin A/C staining also

slightly increases with OGT overexpression, suggesting that OGT dose may directly

correlate with lamin A/C abundance. Likewise, immunoblotting shows the slight increase

in OGT protein as well as the increase in lamin A/C abundance (Figure 3.2C). With

quantitative mass spectrometry (TMT) we were able to determine that the increase in

protein abundance in the XY OGT OE is very small (Figure 3.2D). The Log2-fold

change of OGT in the OGT OE cells compared to the WT XY cells is only about 0.1,

indicating that the OGT transgene is lowly expressed and/or silenced in the OE cells.

Lamin A/C also had a small increase in the OGT OE cells compared to WT XY, a

log2fold change of about 0.2. The minimal variability in the levels of OGT with both

overexpression and protein degradation is consistent with previous data showing that

OGT homeostasis is highly regulated(Lin et al., 2021).

Figure 3.2 *Overexpression of OGT in XY mEScs is silenced.* (A) Immunofluorescence staining of OGT and lamin A in XX, XY, and XY mESCs with an extra copy of OGT inserted (OGT+). (B) Nuclear intensity per unit area quantitation of the OGT staining in (A). (C) Nuclear intensity per unit area quantitation of the lamin A/C staining in (A). Data represents two independent replicates (D) immunoblot of XY and OGT+ cell lines showing a slight increase in OGT protein levels and lamin A/C protein levels in the OGT+ cells. (E) TMT quantitation of OGT and lamin A levels in XX, XY, and OGT+ cells. * $p < 0.05$, ** $p < 0.01$, *** $p < 0.001$, **** $p < 0.0001$

Discussion

OGT expression is very tightly regulated in ESCs(Bond & Hanover, 2015; Tan et al., 2020). Genetic perturbations to OGT expression in both XX and XY mESC lines results in minimal changes in protein abundance due to regulatory mechanisms in place to maintain OGT homeostasis. OGT expression is also highly regulated in other systems – causing previous work to rely on conditional knockouts and small molecule inhibitors to study OGT defects(Keembiyehetty et al., 2015).

Chapter 4

Lamin A Knockout does not affect XX mESC differentiation or XCI

Introduction

Lamin A was previously thought to be nearly undetectable in ESCs(Constantinescu et al., 2006). During differentiation, lamin A expression increases and is easily detectable in most differentiated cells(Burke & Stewart, 2013; Constantinescu et al., 2006). Additional studies have been able to detect lamin A in XY mESCs, but at very low levels compared to MEFs(Eckersley-Maslin et al., 2013).

In contrast to previous work with ESCs, we have found that lamin A/C is abundant and easily detected in XX mESCs. Most mESC studies utilize XY cells, so this contrast in XX vs XY expression went unnoticed. XX and XY mESCs are developmentally similar, except that XX cells must undergo XCI(Maduro et al., 2016; Schulz et al., 2014). While there is extensive research about the process by which the X_i is silenced, there are remaining questions surrounding XCI – How does a cell know it has two X chromosomes? And how does the cell choose which X chromosome to inactivate? It is possible proteins that are highly abundant in XX mESCs compared to XY mESCs could play a role in answering these questions.

We predicted that the abundance of lamin A in XX mESCs is necessary for successful silencing of the X-chromosome. To test this, we knocked out lamin A in XX mESCs and performed RNA fluorescence in situ hybridization (FISH) and RNAseq to detect any changes in XCI. We found that knockout of lamin A in XX mESCs did not have any impact on XCI or differentiation.

Methods

CRISPR Genome Editing

XX-lamin A KO mESCs were derived from LF2 XX mESCs using non-homologous end joining CRISPR/Cas9 genome editing. One guide RNA was selected in the first coding exon, exon 1 of *lmna.* (*Supplementary Table S5*). The guide RNA was cloned into the px459-Cas9-2A-GFP plasmid using published protocols(Ran et al., 2013). The plasmid was transfected into LF2 mESCs using FuGENE HD (Promega) according to the manufacturer's protocol. After two days, cells were treated with 1 μM puromycin to select for clones that are expressing the machinery from the px459 plasmid. Cells were then single cell sorted, so knockouts were propagated from a single cell. Lamin A knockouts were identified by sequencing of each allele (Table S6) which identified indels and point mutations. Protein loss was confirmed by immunoblot.

mEpiLC Differentiation

Cells that were grown in mESC media were transitioned into 2i media consisting of N2B27 media (DMEM/F12, neurobasal media, 2mM L-glutamine, 0.1mM 2-mercaptoethanol, 100X N2 supplement, 50X B27 supplement) and supplemented with 3mM CHIR99021, 1mM PD0325901, and recombinant leukemia inhibitory factor. Tissue-culture dishes were incubated with Geltrex (Gibco) or Matrigel (Corning) diluted in DMEM/F12 media for 30 minutes at 37 ºC and replaced with N2B27 media supplemented with 10ng/mL FGF2 and 20ng/mL Activin A (mEpiLC media). The cells were cultured in mEpiLC media for five days, replacing the media every day.

RNAseq

RNA was extracted using the Qiagen Mini RNeasy Kit (Qiagen 74106). The
integrity of total RNA was checked on Fragment Analyzer (Agilent, Cat. No. DNF-472),
only RNA with RQN number of above 6 was used for library construction. The starting
quantity of 30-100ng of total RNA was used according to vendor instructions with
Universal plus mRNA with Nu Quant (TECAN, Cat. No. 0520), with noted changes to
the protocol as follows: First, the Poly(A) Selection step was omitted; Second, we
started with RNA Fragmentation and used QIAseq FastSelect −rRNA/Globin Kit
(Qiagen, Cat. No. 335377) to remove rRNA and/or globin from the RNA samples as
follows: 0.1ul of each FastSelect Globin and/or 0.1ul of FastSelect rRNA was mixed in
1ul of 1X Fragmentation Buffer; 1ul of this mix was then added to mix of 10ul of total
RNA and 10ul of 2X Fragmentation Buffer; RNA was then fragmented/probed using the
following thermalcycler program: 94 °C/3min, 75 °C/2min, 70 °C /2min, 65 °C/2min,
60 °C/2min, 55°C/2min, 37 °C/5min, 25 °C/5min, 10 °C/hold. After the rRNA/globin
depletion step, the Universal plus mRNA with Nu Quant protocol was followed
according to vendor instructions starting with First Strand cDNA Synthesis step but
skipping the optional steps of AnyDeplete and NuQuant. Final library PCR amplification
was 15 cycles. After library completion, individual libraries were pooled equally by
volume, and quantified on Fragment Analyzer (Agilent, Cat. No. DNF-474). Quantified
library pool was diluted to 1nM and sequenced on MiniSeq (Illumina, Cat. No. FC-420-
1001) to check for quality of reads. Finally, individual libraries were normalized
according to MiniSeq output reads of protein coding genes, corrected for ribosomal,

mitochondrial, and globin reads, and were sequenced on NovaSeq S4 PE100 (Illumina, Cat. No. 20028312)

RNAseq Analysis

Sequencing analysis was performed based on previously established protocols (Dündar et al., 2019; Marin et al., 2024). Raw sequencing files were trimmed using cutadapt (M. Martin, 2011), and then mapped to the GENCODE primary assembly M30 release of the mouse genome (GRCm39) using STAR (Dobin et al., 2012). Bam files were indexed with SAMtools (Danecek et al., 2021), and then the featureCounts (Liao et al., 2014) package and GENCODE M30 primary annotation file were used to generate a read counts table. The read counts table was then input into DESeq2 (Love et al., 2014) to normalize counts, perform differential expression analysis, and generate MA plots. Additional comparisons of differential genes were done in R.

RNA FISH

RNA FISH was performed using directly labeled double-stranded DNA probes, as previously described(Mlynarczyk-Evans et al., 2006). Primers used to generate the Xist probe were previously published (E. A. Martin et al., 2021) . COT-1 FISH was carried out using labeled mouse COT-1 DNA (Invitrogen). Imaging was done on an Olympus BX60 microscope using a 100X objective. For quantification, over 100 nuclei were scored per experiment and graphed in Prism.

Results

Knockout of lamin A in XX mESCs

To test the role of lamin A in XX mESCs, we first knocked out lamin A. We transfected 2 plasmids both containing the Cas-9 machinery and each with a different lamin A guide RNA inserted into the plasmid's gRNA scaffold(Ran et al., 2013). After selection, immunoblots confirmed loss of lamin A protein along with one clone that lost emerin protein as well (Figure 4.1A). Immunofluorescence shows that lamin A is no longer detectable at the nuclear periphery in the KO cells and emerin is less peripherally enriched in the lamin A KO (Figure 4.1B-D). Next, we checked for gene expression changes with RNAseq. Only 99 differentially expressed genes were identified in the RNAseq and none of them indicated a large regulatory role for lamin A (Figure 4.1E).

Figure 4.1 *Validation of lamin A KO in XX mESCs.* (A) Immunoblot showing loss of protein in lamin A KO XX mESCs, along with loss of emerin in one *Lmna* KO clone. (B) Immunofluorescence showing loss of lamin A/C staining in lamin A KO cell lines. (C) Nuclear intensity per unit area quantification of lamin A/C staining in (B). (D) Nuclear intensity per unit area quantification of emerin staining in (B). (E) MA plot of differentially expressed RNAs in WT vs lamin A KO cells. Only 99 genes were differentially expressed in total. **** p < 0.0001, ns = not significant

Lamin A KO has no effect on Xist RNA coating the X_i

To determine if lamin A KO XX mESCs have defects in XCI, we differentiated the

cells for 5 days into epiblast-like cells (mEpiLC). Differentiated cells were probed with

Xist RNA to visualize the inactive X chromosome and *Cot*1 to see actively transcribed

genes. In the amin A KO cells, we see similarly compacted Xs with the *Xist* probing as

we do with WT XX mESCs (Figure 4.2). Similarly, *Cot*1 staining shows a void in the

signal which overlaps with the Xist staining. The lack of *Cot1* staining indicates a lack of

active transcription, which is consistent with successful silencing of the X_i (Figure 4.2).

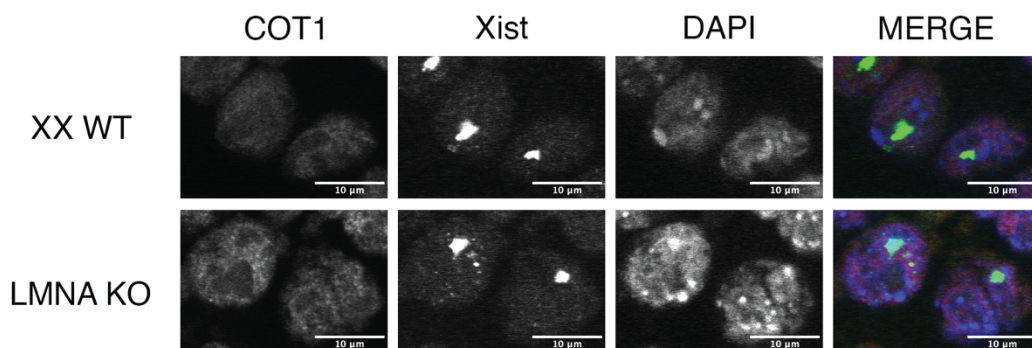

Figure 4.2 *Lamin A Ko cells coat the X_i with Xist similarly to WT XX mESCs.* RNA FISH of *Xist* and *Cot1* on 5 day differentiated XX and XX lamin A KO mEpiLCs. Xist clouds look compact and peripheral in both the WT and lamin A KO cells.

Lamin A KO does not affect gene expression after differentiation

RNAseq comparison of lamin A KO cells at day 0 compared to day 5 of differentiation showed a decreased in pluripotency markers and an increase in epiblast markers (Figure 4.3A). These gene expression changes are similar to those of differentiated WT XX mESCs. Additionally, RNAs that are important for the regulation of XCI, including Xist and Tsix, are upregulated and downregulated respectively which matches WT expression (Figure 4.3C). Looking specifically at the gene expression of X-linked transcripts (Figure 4.3C), the total proportion of X-linked genes that were differentially expressed between WT and lamin A KO cells are similar. Total transcripts that were differentially expressed in an mEpiLC state is even smaller than the mESC state – down to 37 from 99. This suggests that XCI is properly silencing the X_i in these lamin A KO cells and that lamin A KO minimally effects the cell.
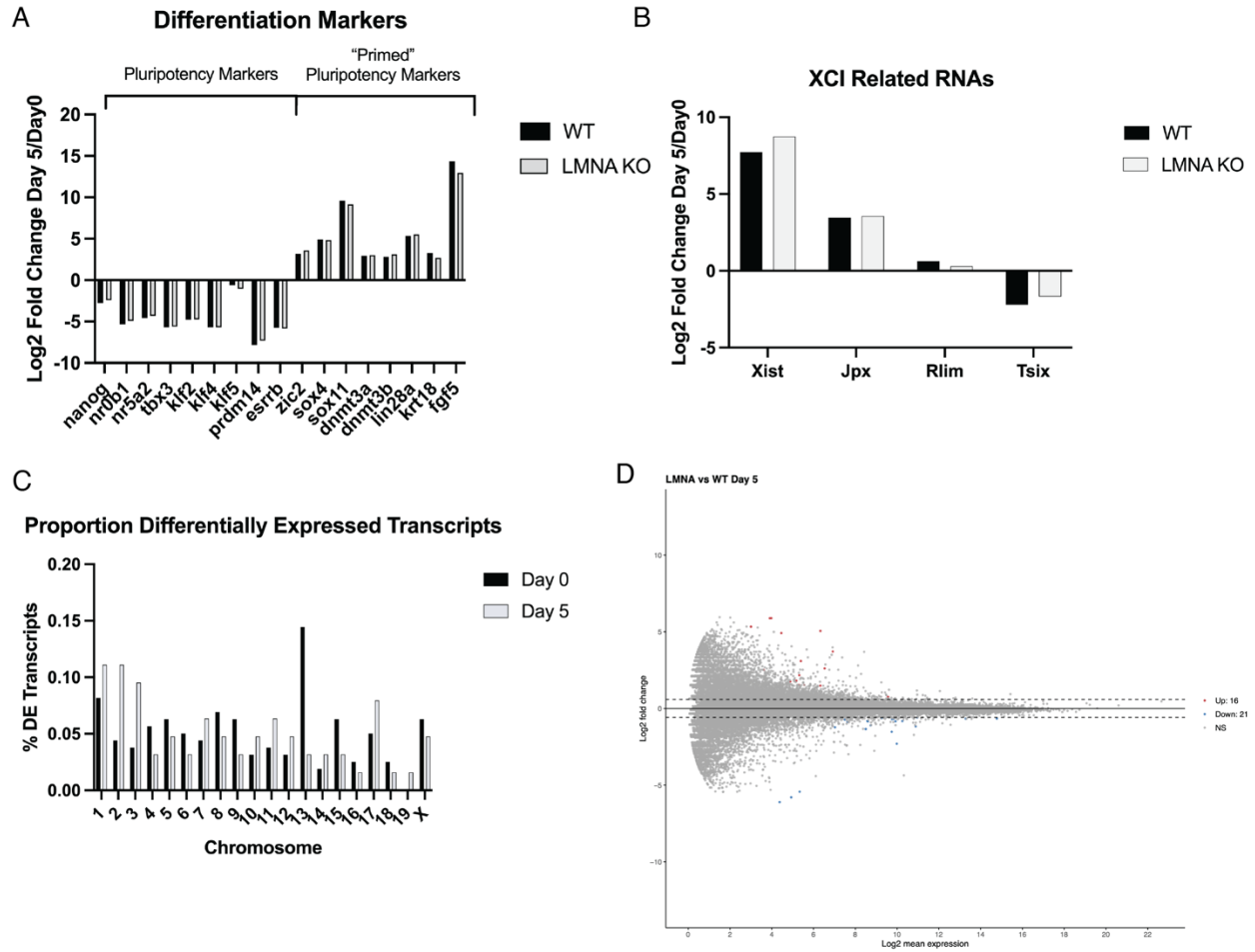
Figure 4.3 *RNAseq analysis of lamin A KO mEpiLCs* (A) Log2-fold changes in expression of differentiation markers from day 5 to day 0. (B) Log2-fold change in expression of XCI related RNAs from day 5 to day 0. (C) Proportion of differentially expressed transcripts from WT to lamin A KO cells on day 5 and day 0. (D) MA plot of lamin A KO vs WT differential gene expression showing only 16 upregulated genes and 21 downregulated genes.

Discussion

Our results suggest that lamin A is not necessary for early development of XX mESCs or XCI, thus an explanation for the higher levels of lamin A in XX mESCs remains unknown.

One possibility is that the lamin A in XX mESCs increases nuclear rigidity. Lamin A is specifically linked to higher stiffness in the nucleus (Burke & Stewart, 2013; Dittmer & Misteli, 2011; Gruenbaum & Foisner, 2015; Schreiber & Kennedy, 2013) , so it is likely that the XXmESC nuclei are much stiffer than the XY mESC nuclei, which could give an advantage in early development.

Previous work has also shown that lamin A KO increases the mobility of transposable elements (TEs) (Marin et al., 2024). XY cells may have more movement of transposable elements than the XX mESCs. The downstream functions of more mobile TEs is unknown but may be able to alter genome reorganization.

Further research into the role of lamin A in these XX mESCs may shed light on new regulatory roles of the nuclear lamina and provide insight into the specific role of lamin A in the larger lamina meshwork.

Chapter 5

O-GlcNAc modified emerin is not required for XX mESC differentiation

Introduction

Emerin (EMD) is a component of the nuclear periphery that interacts with the nuclear lamina (Berk et al., 2014; Lee et al., 2001). It requires lamin A for proper localization to the periphery and directly interacts with lamin A via a lamin binding domain(Lee et al., 2001) and a ternary structure between its LEM domain, barrier to autointegration factor (BAF), and the Ig fold domain of lamin A(Samson et al., 2018). Emerin is X-linked and more abundant in XX mESCs compared to XY mESCs, due to XX mESCs having two active X chromosomes. Mutations in EMD can lead to Emery-Dryfuss Muscular Dystrophy, a condition that largely affects skeletal muscle and motor function(Berk, Tifft, et al., 2013; Koch & Holaska, 2014). In WT cells the function of emerin is poorly understood. It has been linked to many pathways, including cell-cell junction interactions, Wnt signaling, and chromatin organization (Koch & Holaska, 2014), however its specific roles are not well understood.

Similarly to the high levels of lamin A in XX mESCs, we predicted that the high levels of X-linked EMD at the nuclear periphery may assist in XCI regulation. To test the role of EMD in XCI, we studied the effects of emerin knockout in both XX mESCs and XX mEpiLCs. We found that there are minimal effects of emerin knockout in both cell states, and emerin is likely not involved in XCI regulation.

Methods

Experiments were conducted according to the methods in Chapters 2 and 4. Two guide RNAs were selected for *Emd* knockout, one in exon 2 and the other in exon 4, 631bp apart *(Supplementary Table S6)* and the gRNA plasmids were co-transfected into the XX mESCs.

Results

Emerin is highly abundant in XX mESCs

Emerin is expressed at high levels in XX mESCs compared to XY mESCs. Immunofluorescence staining shows enrichment of emerin at the nuclear periphery of XX mESCs along with staining just outside of the nucleus in the ER (Figure 5.1 A and B). Whole cell immunoblot confirms the increased abundance of emerin in XX mESCs (Figure 5.1C). To more quantitatively explore emerin protein levels in XX and XY mESCs, we performed TMT. In comparison of XX vs XO and XX vs XY datasets, we see that emerin's high expression correlates positively to number of X-chromosomes (Figure 5.1F). This correlation is expected as emerin is X-linked. *O*-GlcNAc enriched SiLAC also shows that emerin is highly *O*-GlcNAc modified in XX mESCs (Figure 5.1D). The unstructured lamin binding domain of EMD contains a serine rich region that is 2.5 fold more *O*-GlcNAcylated in XX compared to XY cells (Figure 5.1E).
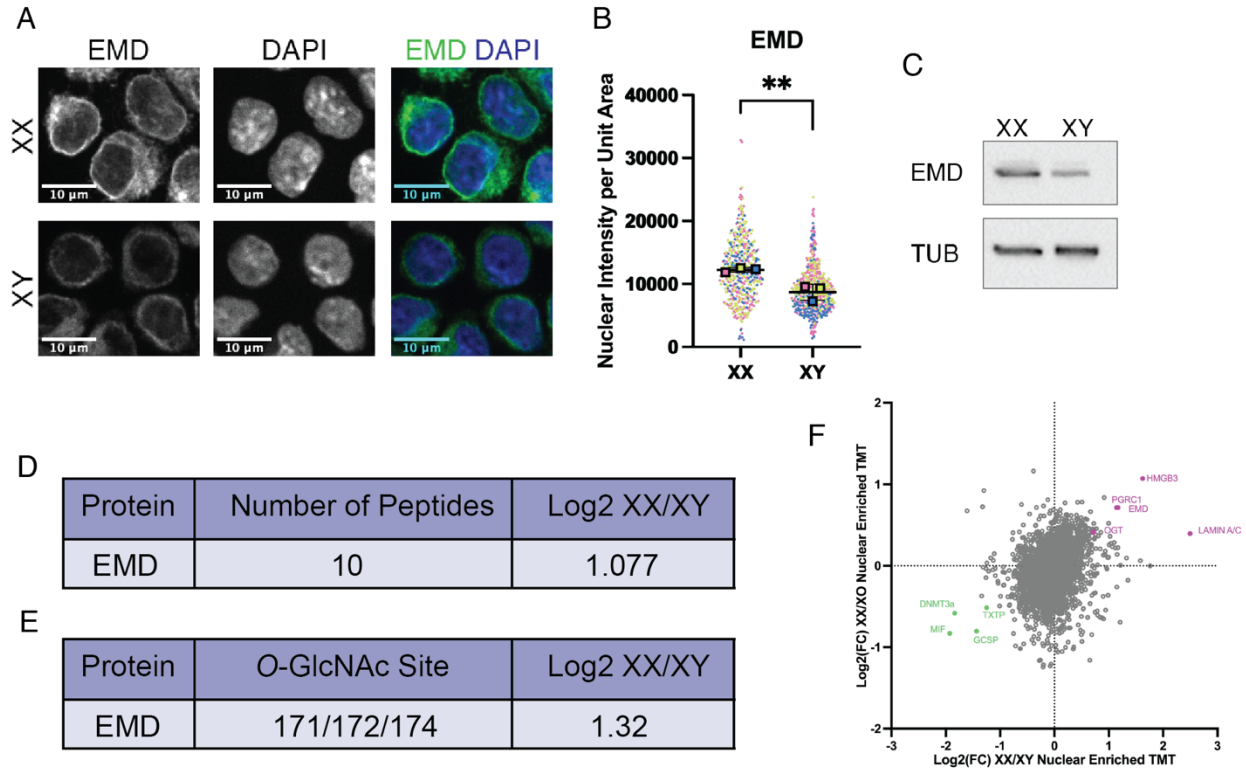
A

EMD | DAPI | EMD DAPI

XX

XY

10 µm

B

EMD

**

Nuclear Intensity per Unit Area

40000

30000

20000

10000

0

XX   XY

C

XX   XY

EMD

TUB

D

Protein	Number of Peptides	Log2 XX/XY
EMD	10	1.077

E

Protein	O-GlcNAc Site	Log2 XX/XY
EMD	171/172/174	1.32

F

Log2(FC) XX/XO Nuclear Enriched TMT

HMGB3
PGRC1
EMD
OGT
LAMIN A/C
DNMT3a
TXTP
MIF
GCSP

Log2(FC) XX/XY Nuclear Enriched TMT

Figure 5.1 *Emerin is highly expressed in XX mESCs* (A) Immunofluorescence staining of emerin on XX and XY mESCs. Cells were imaged on a Nikon Ti inverted fluorescence microscope with CSU-22 spinning disk confocal. Representative middle slices were chosen. Scale bar is 10nm. (B) Quantitation of nuclear intensity per unit area of emerin fluorescence in (A). Data represents quantitation of 3 independent experiments indicated by color. (C) Western blot of XX and XY mESC whole cell extracts. 20µg nuclear protein loaded per lane. TUB represents loading control. (D) Table of total protein abundance of emerin and its fold change (XX/XY) quantified from SILAC dataset. (E) Table of identified *O*-GlcNAcylated peptide in emerin and its fold change (XX/XY). (F) TMT results graphed as correlation plot of log2 fold change of detected proteins in XX vs XY nuclei (x-axis) and XX vs XO nuclei (y-axis). ** $p < 0.01$

Loss of OGT activity does not affect emerin abundance or distribution

Next, we explored the potential regulatory relationship between OGT and emerin, due to the identified *O*-GlcNAc sites in the unstructured domain of emerin. We used a pharmacological inhibitor, OSMI-4, to inhibit OGT and measured emerin protein levels and localization by immunofluorescence. Emerin abundance increases slightly but localization around the nuclear periphery is unaffected by the inhibition of OGT (Figure 5.2A and B). In contrast, immunoblotting shows that emerin abundance stays constant with OSMI-4 treatment (Figure 5.2C), suggesting that *O*-GlcNAc modification of emerin does not play a role in its expression level or distribution around the nuclear periphery.
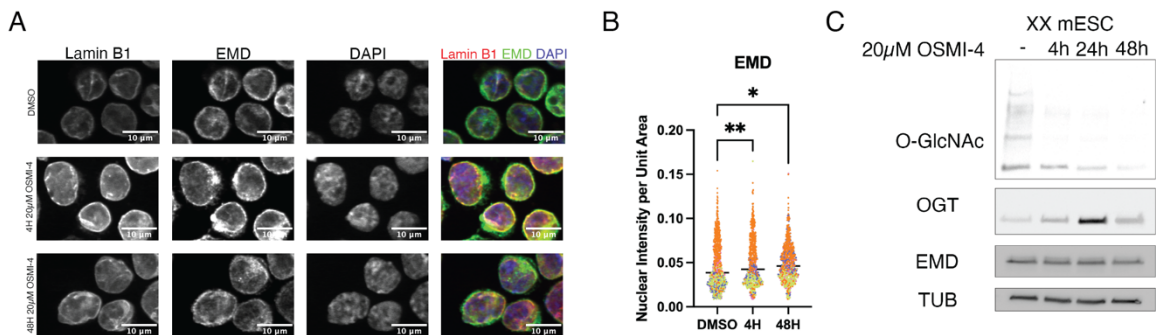
Figure 5.2 *OSMI-4 inhibition has no effect on emerin abundance and distribution* (A) Immunofluorescence staining of emerin and lamin B1 on XX mESCs treated with 20µM OSMI-4 for 4 or 48 hours or with carrier DMSO for 48 hours. Cells were imaged on a Nikon Ti inverted fluorescence microscope with CSU-22 spinning disk confocal. Representative z-slices were chosen. Scale bar is 10nm. (B) Quantitation of nuclear fluorescence intensity per unit area of emerin signal represented in (A). Data represents quantitation of 4 independent experiments indicated by color. (C) Western blot showing changes in overall *O*-GlcNAcylation, OGT, and emerin abundance after treatment with 20µM OSMI-4 or carrier DMSO for 4, 24, and 48 hours. * $p < 0.05$, ** $p < 0.01$

Emerin Knockout does not alter gene expression in XX mESCs

To determine the function of high levels of emerin in XX mESCs, we knocked out emerin from XX mESCs using a CRISPR-Cas9 gene editing system. The emerin KO mESC line was genotyped by PCR and lost protein was confirmed by immunofluorescence and immunoblot (Figure 5.3A-C). To assess the gene regulation role of EMD, RNAseq was performed on EMD KO and WT XX mESCs. In pluripotent cells, very few (<100) genes were differentially expressed between EMD KO and WT XX mESCs (Figure 5.3D). Most of these differentially expressed genes are part of cellular trafficking pathways, but genes related to emerin's predicted functions including Beta-catenin and Lap2 were unaffected by emerin KO.
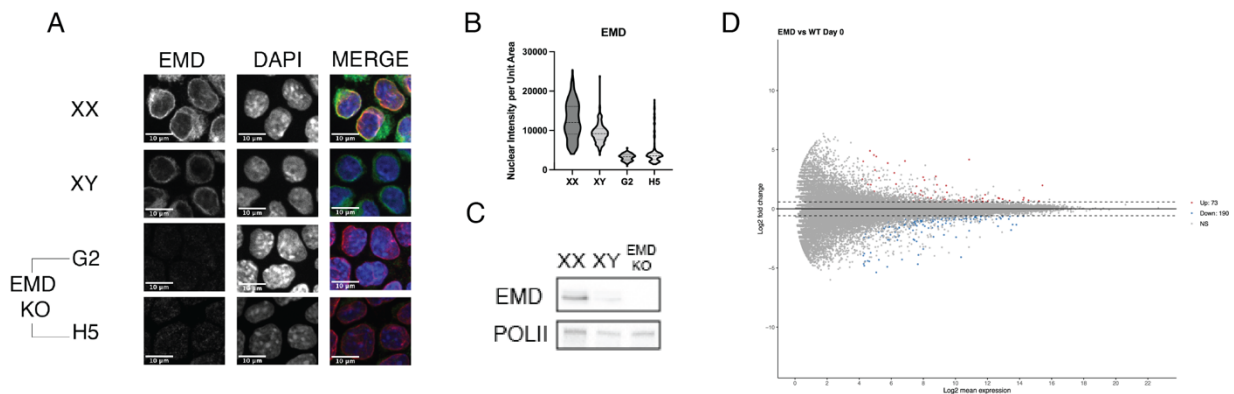
Figure 5.3 *Effects of emerin KO on XX mESCs* (A) Immunofluorescence staining of emerin on XX, XY, and XX emerin KO mESCs. Cells were imaged on a Nikon Ti inverted fluorescence microscope with CSU-22 spinning disk confocal. Representative middle slices were chosen. Scale bar is 10nm (B) Quantitation of nuclear fluorescence intensity per unit area of emerin signal represented in (A). (C) Western blot of XX, XY, and XX emerin Ko mESC whole cell extracts. 20µg nuclear protein loaded per lane. POLII represents loading control. (D) MA plot of differentially expressed genes in EMD KO vs WT XX mESCs generated in r using DEseq. 263 genes were differentially expressed between the two cell types.

Effects of emerin KO on XCI in mEpiLCs

As there are no major changes in gene expression due to emerin loss in the mESC state, we wanted to test the role of emerin through differentiation. We differentiated WT and emerin KO cells for 5 days into mEpiLCs which have undergone XCI. Morphologically, loss of emerin does not appear to affect differentiation. To assess basic structure of the X_i we stained the differentiated cells for H3K27me3 and RNAP2. EMD (Figure 5.4A). In both the EMD KOs and WT XX mESCs some inactive Xs have aberrant morphology, either larger than normal or elongated like a comet. There is no difference, however, in the proportion of aberrant X_is in WT compared to emerin KO cells (Figure 5.4B), suggesting that emerin does not play a role in XCI regulation.
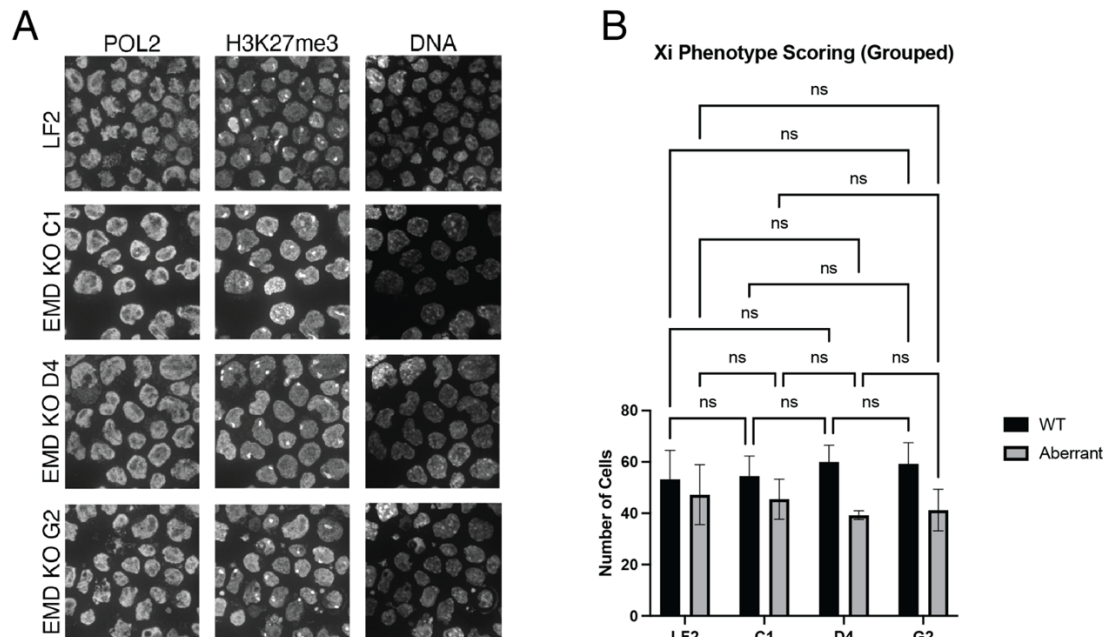

Figure 5.4 *Effects of emerin KO on XCI.* (A) Immunofluorescence staining of RNA POLII and H3K27me3 on WT and emerin KO XX mEpiLCs. Cells were imaged on a Nikon Ti inverted fluorescence microscope with CSU-22 spinning disk confocal. Representative middle slices were chosen. (B) Scoring of aberrant vs WT X_i phenotypes based on the H3K27me3 staining in (A). ns = not significan

Emerin KO does not alter gene expression in mEpiLCs

To quantitatively determine effects of emerin KO on gene expression, RNAseq was done to compare gene expression after the 5-day mEpiLC differentiation. Overall, very few genes were differentially expressed in emerin KO mEpiLCs compared to WT mEpiLCs (Figure 5.5A). To determine successful differentiation, we looked at expression levels of pluripotency markers and mEpiLC markers. In the emerin KOs common pluripotency markers decreased with differentiation while mEpiLC markers increased, similarly to WT XX mESCs (Figure 5.5B). Additionally, XCI related RNAs, Xist and Tsix, increase and decrease in the KOs similarly to WT cells (Figure 5.5C). Finally, there are very few X-linked genes that are differentially expressed between the day 5 EMD KOs and the day 5 WT XX mESCs (Figure 5.5D-E), indicating that X-chromosome silencing is likely occurring normally in the EMD KOs
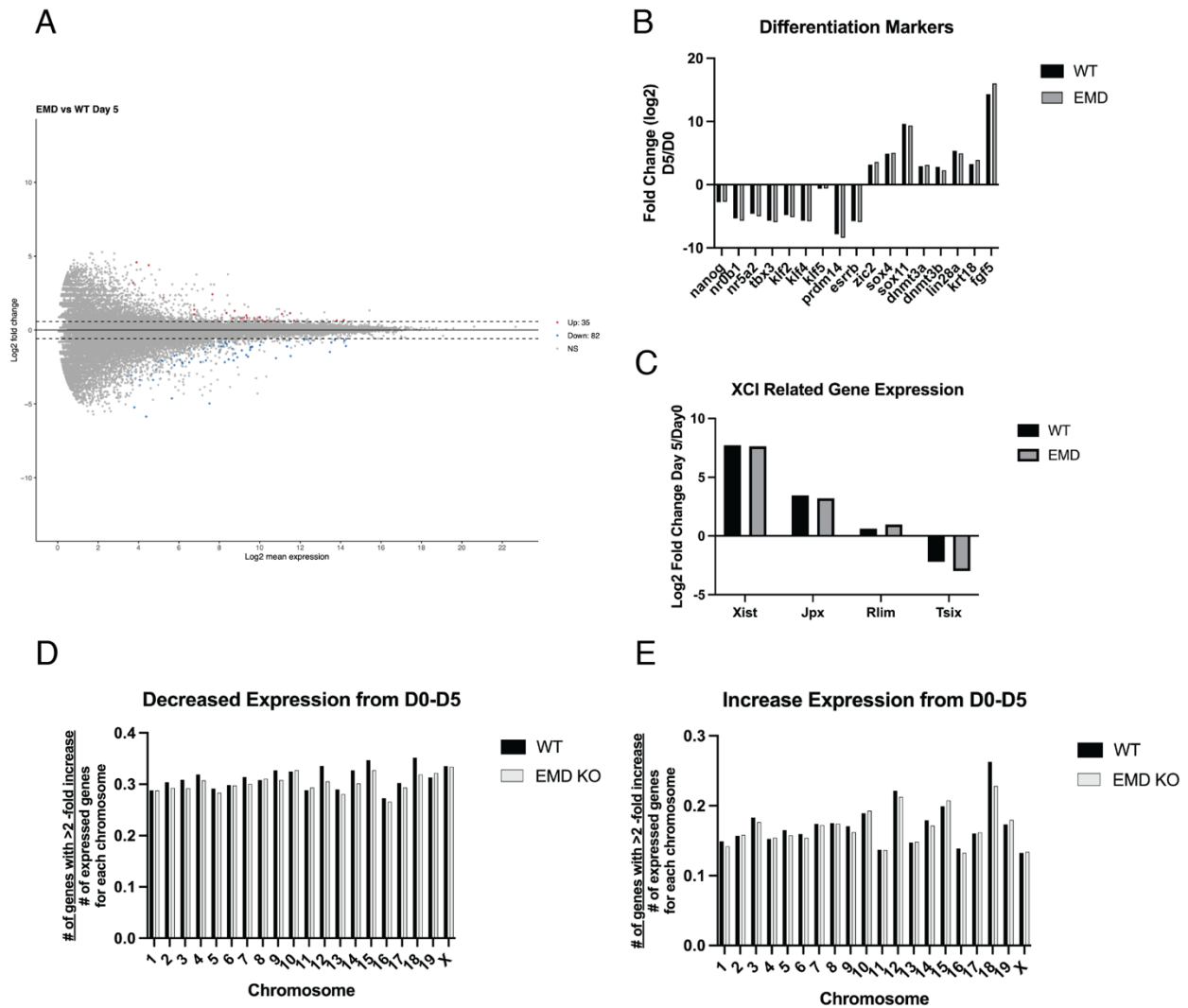
Figure 5.5 *Gene expression changes in WT vs emerin KO mEpiLCs* (A) MA plot of emerin KO vs WT differential gene expression in mEpiLCs showing only 36 upregulated genes and 82 downregulated genes. (B) Log2-fold changes in expression of differentiation markers from day 5 to day 0. (C) Log2-fold change in expression of XCI related RNAs from day 5 to day 0. (D) Proportion of decreased transcripts from WT to lamin A KO cells on day 5 and day 0. (E) Proportion of increased transcripts from WT to lamin A KO cells on day 5 and day 0.

Discussion

Our results indicate that there is no effect of emerin KO on the XX mESCs. This negative result could be the result of a few scenarios. First, as shown by previous work, emerin KO mice can grow into adulthood with minimal negative phenotypes while humans with effective emerin KO suffer disease phenotypes. There is likely some redundancy or other protective mechanism in mice that prevents or obscures more extreme phenotypes from emerin KO in our mESCs. Repeating this knockout study utilizing human stem cells rather than mouse stem cells could allow us to see a more profound phenotype.

An additional confounding factor in this line of experimentation is allele specificity. The bulk RNAseq experiment was done on a population of cells and allele-specific transcriptional levels cannot be parsed from the dataset as there are no chromosome specific labels. It could be possible that gene expression changes from the X-chromosome after XCI in EMD KOs are not measurable in this dataset due to upregulation of the genes on the active X-chromosome. Additionally, specific alleles may have unique expression patterns, which we cannot see in this bulk dataset. Allele specificity can also provide insight into X-chromosome choice. If EMD is necessary for choice of an X-chromosome to silence, then allele specific sequencing would allow us to determine if *O*-GlcNAc modification of EMD is required to label the Xi

Altogether, our data show that emerin is not necessary for differentiation from mESCS to mEpiLCs and is likely not involved in XCI regulation. The specific mechanisms by which emerin functions in the various pathways it has been implicated in remain to be understood.

Appendix

Supplemental Figures and Tables

Associated with Chapter 2
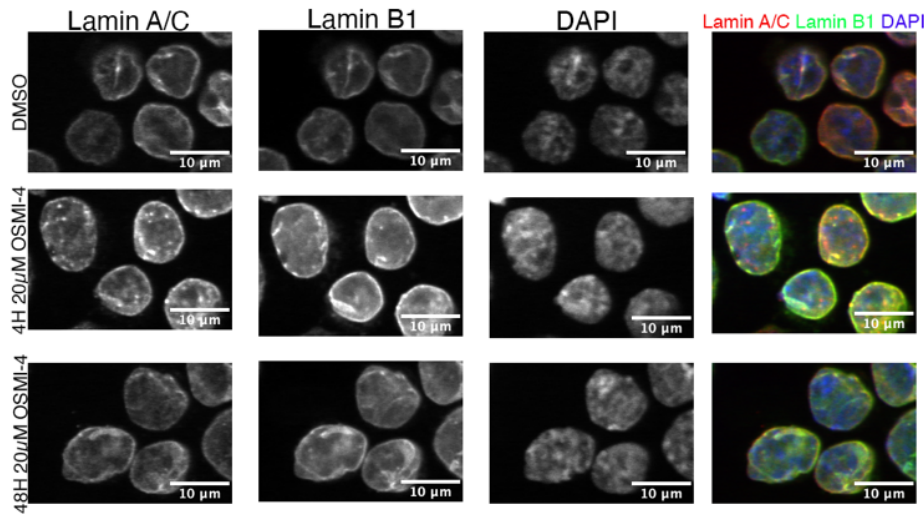
Figure S1 *Lamin A localization after OSMI-4 treatment*
Immunofluorescence staining of lamin A/C, lamin B1, and DAPI on XX mESCs treated with 20µM OSMI-4 for 4 or 48 hours or with carrier DMSO for 48 hours. Cells were imaged on a Nikon Ti inverted fluorescence microscope with CSU-22 spinning disk confocal. Representative middle slices were chosen. Scale bar is 10nm. Lamin A/C and lamin B1 co-localize at the nuclear periphery.
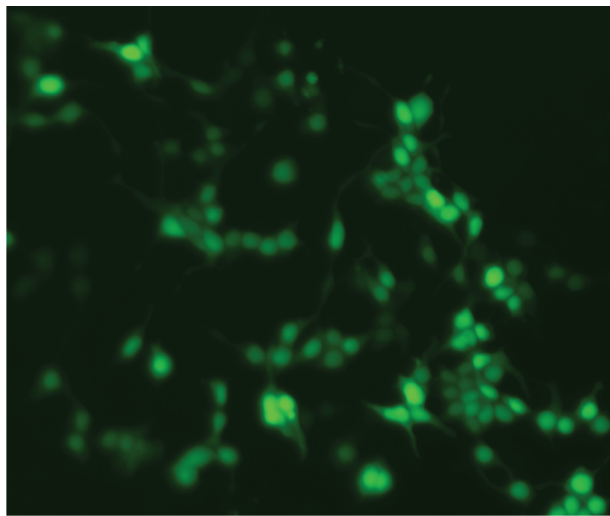
GFP-NLS-LMNA Tail (WT)

Figure S2 *Distribution of overexpressed lamin A tail in HEK 293T cells*
293T cells containing the WT lamin A tail construct were induced with 1µM Dox for 24hrs and imaged on an Echo Revolve fluorescent microscope. Distribution of lamin A Tail peptide is primarily in the nucleus, with some lamin A tail also in the cytoplasm

acccagtccgccctgagcaaagaccccaacgagaagcgcgatcacatggtcctgctggagttcgtgaccgccgccgggatcactctcggcatggacgagctgtacaa
tgggtcaggcgggactcgtttctggggttgctcttcgcgctagtgtaccaggacgacctcaagcactggcggcggcccctagtgagagccgtacctgctcgacatgtt

GFP

| 10 | 20 | 30 | 40 | 50 | 60 | 70 | 80 | 90 | 100 |

gACCAAAAAGCGCAAACTGGAGTCCCGCAGCTACCGCAGTGTGGGGGGCAGTGGGGGTGGCAGCTTCGGGGACAATCTGGTCACCCGCTCCTACCTCCTGGGCAACT
cTGGTTTTTCGCGTTTGACCTCAGGGCGTCGATGGCGTCACACCCCCCGTCACCCCCACCGTCGAAGCCCCTGTTAGACCAGTGGGCGAGGATGGAGGACCCGTTGA

NLS   Lamin A Tail

| 110 | 120 | 130 | 140 | 150 | 160 | 170 | 180 | 190 | 200 | 210 |

CCAGCCCCCGAACCCAGAGCCCCCAGAACTGCAGCATCATGTAAactagtagaccacctcccctgcgagctaagctggacagccaatgacgggtaagagagtgacat
GGTCGGGGGCTTGGGTCTCGGGGGTCTTGACGTCGTAGTACATTtgatcatctggtggaggggacgctcgattcgacctgtcggttactgcccattctctcactgta

Lamin A Tail

| 220 | 230 | 240 | 250 | 260 | 270 | 280 | 290 | 300 | 310 | 320 |

ttttcactaacctaagacaggagggccgtcagagctactgcctaatccaaagacgggtaaaagt
aaaagtgattggattctgtcctcccggcagtctcgatgacggattaggtttctgcccattttca

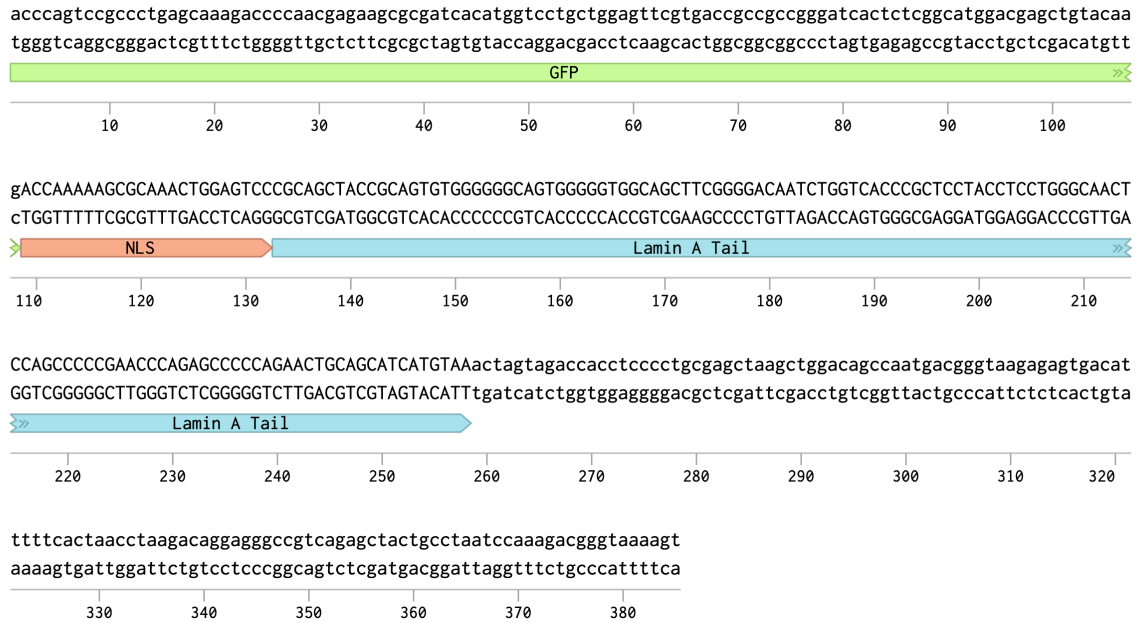| 330 | 340 | 350 | 360 | 370 | 380 |

Figure S3 *gBlock (GFP-NLS-lamin A Tail) for HiFi Assembly of XLone-GFP-lamin A Tail*

Table S1 *Primary Antibodies*

Antigen	Manufacturer	Cat. #	Dilution IF	Dilution WB
lamin A/C	Santa Cruz	sc-376248	1:100	1:1000
O-GlcNAc	Abcam	ab2739	1:100	1:1000
OGT	Cell Signaling Technology	D1D8Q	1:100	1:1000
GFP	Proteintech	pabg1	NA	1:1000
emerin	Proteintech	10351-1-AP	1:100	1:1000
α-Tubulin	Sigma	T5168	NA	1:2000
GAPDH	Genetex	GTX637966	NA	1:5000

Table S2 *Secondary Antibodies*

Antibody	Manufacturer	Cat. #	Dilution
568 AlexaFluor Goat anti Rabbit 2º	LifeTechnologies	A11011	1:1000
488 AlexaFluor Goat anti Mouse 2º	LifeTechnologies	A11029	1:1000
HRP-Conjugated Goat anti Rabit 2º	VWR	RL611-1302	1:5000
HRP-Conjugated Goat anti Mouse 2º	VWR	RL610-1302	1:5000
Anti Rabbit 2º (DyLight680 Conjugate)	Cell Signaling Technology	5366S	1:5,000 – 1:20,000
IRDye 800CW Goat anti Mouse 2º	LiCor	926-32210	1:5,000 – 1:20,000

Table S3 *Table of variable modifications used in the SiLAC mass spectrometry analysis*

Acetyl (Protein N-term)	HexNAc4Hex6 (N) - Rare - Motif 0 N[^P][ST]
Acetyl+Oxidation (Protein N-term M)	HexNAc4Hex6Fuc (N) - Rare - Motif 0 N[^P][ST]
Gln->pyro-Glu (N-term Q)	HexNAc4Hex6Fuc2 (N) - Rare - Motif 0 N[^P][ST]
HexNAc (N) - Rare - Motif 0 N[^P][ST]	HexNAc4Hex6SA (N) - Rare - Motif 0 N[^P][ST]
HexNAc (ST)	HexNAc4Hex6SAOx2 (N) - Rare - Motif 0 N[^P][ST]
HexNAc2 (N) - Rare - Motif 0 N[^P][ST]	HexNAc4Hex7 (N) - Rare - Motif 0 N[^P][ST]
HexNAc2Fuc (N) - Rare - Motif 0 N[^P][ST]	HexNAc5Hex3 (N) - Rare - Motif 0 N[^P][ST]
HexNAc2Hex (N) - Rare - Motif 0 N[^P][ST]	HexNAc5Hex3Fuc (N) - Rare - Motif 0 N[^P][ST]
HexNAc2Hex (ST) - Rare	HexNAc5Hex3FucSA (N) - Rare - Motif 0 N[^P][ST]
HexNAc2Hex10 (N) - Rare - Motif 0 N[^P][ST]	HexNAc5Hex4 (N) - Rare - Motif 0 N[^P][ST]
HexNAc2Hex2 (N) - Rare - Motif 0 N[^P][ST]	HexNAc5Hex4Fuc (N) - Rare - Motif 0 N[^P][ST]
HexNAc2Hex2 (ST) - Rare	HexNAc5Hex4Fuc2 (N) - Rare - Motif 0 N[^P][ST]
HexNAc2Hex2Fuc (N) - Rare - Motif 0 N[^P][ST]	HexNAc5Hex4FucSA2 (N) - Rare - Motif 0 N[^P][ST]
HexNAc2Hex3 (N) - Rare - Motif 0 N[^P][ST]	HexNAc5Hex4NeuAc (N) - Rare - Motif 0 N[^P][ST]
HexNAc2Hex3Fuc (N) - Rare - Motif 0 N[^P][ST]	HexNAc5Hex4SA (N) - Rare - Motif 0 N[^P][ST]
HexNAc2Hex4 (N) - Rare - Motif 0 N[^P][ST]	HexNAc5Hex5 (N) - Rare - Motif 0 N[^P][ST]
HexNAc2Hex4Fuc (N) - Rare - Motif 0 N[^P][ST]	HexNAc5Hex5Fuc (N) - Rare - Motif 0 N[^P][ST]
HexNAc2Hex5 (N) - Rare - Motif 0 N[^P][ST]	HexNAc5Hex5FucSA (N) - Rare - Motif 0 N[^P][ST]
HexNAc2Hex5Fuc (N) - Rare - Motif 0 N[^P][ST]	HexNAc5Hex5FucSA2 (N) - Rare - Motif 0 N[^P][ST]
HexNAc2Hex6 (N) - Rare - Motif 0 N[^P][ST]	HexNAc5Hex5SA (N) - Rare - Motif 0 N[^P][ST]
HexNAc2Hex6Fuc (N) - Rare - Motif 0 N[^P][ST]	HexNAc5Hex5SA2 (N) - Rare - Motif 0 N[^P][ST]
HexNAc2Hex7 (N) - Rare - Motif 0 N[^P][ST]	HexNAc5Hex6 (N) - Rare - Motif 0 N[^P][ST]
HexNAc2Hex8 (N) - Rare - Motif 0 N[^P][ST]	HexNAc5Hex6Fuc (N) - Rare - Motif 0 N[^P][ST]
HexNAc2Hex9 (N) - Rare - Motif 0 N[^P][ST]	HexNAc5Hex6FucSA (N) - Rare - Motif 0 N[^P][ST]
HexNAc2HexFuc (N) - Rare - Motif 0 N[^P][ST]	HexNAc5Hex6FucSA2 (N) - Rare - Motif 0 N[^P][ST]
HexNAc3Hex3 (N) - Rare - Motif 0 N[^P][ST]	HexNAc5Hex6SA (N) - Rare - Motif 0 N[^P][ST]
HexNAc3Hex3Fuc (N) - Rare - Motif 0 N[^P][ST]	HexNAc5Hex6SA2 (N) - Rare - Motif 0 N[^P][ST]
HexNAc3Hex4 (N) - Rare - Motif 0 N[^P][ST]	HexNAc5Hex6SA3 (N) - Rare - Motif 0 N[^P][ST]
HexNAc3Hex4SA (N) - Rare - Motif 0 N[^P][ST]	HexNAc6Hex7FucSA (N) - Rare - Motif 0 N[^P][ST]
HexNAc3Hex5 (N) - Rare - Motif 0 N[^P][ST]	HexNAc6Hex7SA (N) - Rare - Motif 0 N[^P][ST]
HexNAc3Hex5Fuc (N) - Rare - Motif 0 N[^P][ST]	HexNAc6Hex7SA2 (N) - Rare - Motif 0 N[^P][ST]
HexNAc3Hex5SA (N) - Rare - Motif 0 N[^P][ST]	HexNAc7Hex6SA2 (N) - Rare - Motif 0 N[^P][ST]
HexNAc3Hex5SAOxSAOxAc (N) - Rare - Motif 0 N[^P][ST]	HexNAc7Hex6SA3 (N) - Rare - Motif 0 N[^P][ST]
HexNAc3Hex6 (N) - Rare - Motif 0 N[^P][ST]	HexNAcFuc (N) - Rare - Motif 0 N[^P][ST]
HexNAc3Hex6Fuc (N) - Rare - Motif 0 N[^P][ST]	HexNAcFuc (ST) - Rare
HexNAc3Hex6SA (N) - Rare - Motif 0 N[^P][ST]	HexNAcHex (ST) - Rare
HexNAc3Hex6SA2 (N) - Rare - Motif 0 N[^P][ST]	HexNAcHexFuc (ST) - Rare
HexNAc3Hex7 (N) - Rare - Motif 0 N[^P][ST]	HexNAcHexSA (ST) - Rare
HexNAc3Hex7Fuc (N) - Rare - Motif 0 N[^P][ST]	HexNAcHexSA2 (ST) - Rare
HexNAc4Hex3 (N) - Rare - Motif 0 N[^P][ST]	HexNAcHexSAAc (ST) - Rare
HexNAc4Hex3Fuc (N) - Rare - Motif 0 N[^P][ST]	HexNAcHexSAAc2 (ST) - Rare
HexNAc4Hex4 (N) - Rare - Motif 0 N[^P][ST]	HexNAcHexSAAcSAOxAc (ST) - Rare
HexNAc4Hex4Fuc (N) - Rare - Motif 0 N[^P][ST]	HexNAcHexSAOx (ST) - Rare
HexNAc4Hex4Fuc2 (N) - Rare - Motif 0 N[^P][ST]	HexNAcHexSAOx2 (ST) - Rare
HexNAc4Hex4FucSA (N) - Rare - Motif 0 N[^P][ST]	HexNAcHexSAOxAc2 (ST) - Rare
HexNAc4Hex4SA (N) - Rare - Motif 0 N[^P][ST]	HexNAcHexSAOxSAOxAc (ST) - Rare
HexNAc4Hex5 (N) - Rare - Motif 0 N[^P][ST]	HexNAcHexSASAAc (ST) - Rare
HexNAc4Hex5Fuc (N) - Rare - Motif 0 N[^P][ST]	HexNAcHexSASAOx (ST) - Rare
HexNAc4Hex5Fuc2 (N) - Rare - Motif 0 N[^P][ST]	HexNAcHexSASAOxAc (ST) - Rare
HexNAc4Hex5FucSA (N) - Rare - Motif 0 N[^P][ST]	HexNAcSA (ST) - Rare
HexNAc4Hex5FucSA2 (N) - Rare - Motif 0 N[^P][ST]	HexNAcSAOx (ST) - Rare
HexNAc4Hex5FucSAOx2 (N) - Rare - Motif 0 N[^P][ST]	Label:13C(6) (R) - Label 1
HexNAc4Hex5SA (N) - Rare - Motif 0 N[^P][ST]	Label:13C(6)15N(2) (K) - Label 1
HexNAc4Hex5SA2 (N) - Rare - Motif 0 N[^P][ST]	Met-loss (Protein N-term M)
HexNAc4Hex5SAOx (N) - Rare - Motif 0 N[^P][ST]	Met-loss+Acetyl (Protein N-term M)
HexNAc4Hex5SAOx2 (N) - Rare - Motif 0 N[^P][ST]	Oxidation (M)
HexNAc4Hex5SAOx3 (N) - Rare - Motif 0 N[^P][ST]	Pyro-carbamidomethyl (N-term C)
HexNAc4Hex5SAOxSAOxAc (N) - Rare - Motif 0 N[^P][ST]	

Table S4 *Primers for lamin A tail construct and site directed mutagenesis*

Cell Line	Forward	Reverse
WT lamin A Tail HiFi Assembly	CGAGCTGTACAAGACCAAA AAGCGCAAACTGGAGTCCC GCAGCTACCGCAGTGTGG	TGCGGTAGCTGCGGGA CTCCAGTTTGCGCTTTTTG GTCTTGTACAGCTCGTCCATGCC GA
Mature lamin A Tail	TAAACTAGTAGACCACCTCCC	GTAGGAGCGGGTGACCAG
L647R lamin A Tail	CCGCTCCTACCGACTGGGCAACT	GTGACCAGATTGTCCCCG
T643A lamin A Tail	CAATCTGGTCGCCCGCTCCTACC	TCCCCGAAGCTGCCACCC
S645A lamin A Tail	GGTCACCCGCGCCTACCTCCTGG	AGATTGTCCCCGAAGCTGCC
T643A+S645 A lamin A Tail	CAATCTGGTCGCCCGCGCCTACC	TCCCCGAAGCTGCCACCC
D639A lamin A Tail	CAGCTTCGGGGCCAATCTGGTCAC CC	CCACCCCCACTGCCCCCC
D639A+S645 A lamin A Tail	GGTCACCCGCGCCTACCTCCTGG	AGATTGGCCCCGAAGCTGC
Triple Mutant lamin A Tail	CAATCTGGTCGCCCGCGCCTACC	GCCCCGAAGCTGCCACCC

Table S5 *Guide RNAs and Primers for CRISPR-Cas9 Knockout generation*

Cell Line	Guide(s)	Genotyping Primer F	Genotyping Primer R
Lamin A KO	CACCGCCATGGAGACCCCGTCAC**AGG**TTT	CCTTCAGCTCCTTGAACTCC	TTCACAATGTTGGTTCCTGC
Emerin KO	CACCGCTTTTCGTAGAGCTTGCG**AGG**TTT CACCGGGTATCAGCATCTACAAG**TGG**TTT	TTCACAATGTTGGTTCCTGC	TTGGGGATGCTCAGCAGAAG

References

Babatz, T. D., Spear, E. D., Xu, W., Sun, O. L., Nie, L., Carpenter, E. P. & Michaelis, S. (2021). Site specificity determinants for prelamin A cleavage by the zinc metalloprotease ZMPSTE24. *Journal of Biological Chemistry*, *296*, 100165.

Baker, P. R., Trinidad, J. C. & Chalkley, R. J. (2011). Modification Site Localization Scoring Integrated into a Search Engine*. *Molecular & Cellular Proteomics*, *10*(7), M111.008078.

Barrowman, J., Hamblet, C., Kane, M. S. & Michaelis, S. (2012). Requirements for Efficient Proteolytic Cleavage of Prelamin A by ZMPSTE24. *PLoS ONE*, *7*(2), e32120.

Berk, J. M., Maitra, S., Dawdy, A. W., Shabanowitz, J., Hunt, D. F. & Wilson, K. L. (2013). O-Linked β-N-Acetylglucosamine (O-GlcNAc) Regulates Emerin Binding to Barrier to Autointegration Factor (BAF) in a Chromatin- and Lamin B-enriched "Niche"*. *Journal of Biological Chemistry*, *288*(42), 30192–30209.

Berk, J. M., Simon, D. N., Jenkins-Houk, C. R., Westerbeck, J. W., Grønning-Wang, L. M., Carlson, C. R. & Wilson, K. L. (2014). The molecular basis of emerin–emerin and emerin–BAF interactions. *Journal of Cell Science*, *127*(18), 3956–3969.

Berk, J. M., Tifft, K. E. & Wilson, K. L. (2013). The nuclear envelope LEM-domain protein emerin. *Nucleus*, *4*(4), 298–314.

Bond, M. R. & Hanover, J. A. (2015). A little sugar goes a long way: The cell biology of O-GlcNAc. *Journal of Cell Biology*, *208*(7), 869–880.

Burke, B. & Stewart, C. L. (2013). The nuclear lamins: flexibility in function. *Nature Reviews Molecular Cell Biology*, *14*(1), 13–24.

Chen, C.-K., Blanco, M., Jackson, C., Aznauryan, E., Ollikainen, N., Surka, C., Chow, A., Cerase, 1 Andrea, McDonel, P. & Guttman, M. (2016). Xist recruits the X chromosome to the nuclear lamina to enable chromosome-wide silencing. *Science*.

Chen, C.-K., Chow, A., Lai, M. & Guttman, M. (2017). Response to Comment on "Xist recruits the X chromosome to the nuclear lamina to enable chromosome-wide silencing." *Science*, *356*(6343).

Constantinescu, D., Gray, H. L., Sammak, P. J., Schatten, G. P. & Csoka, A. B. (2006). Lamin A/C Expression Is a Marker of Mouse and Human Embryonic Stem Cell Differentiation. *STEM CELLS*, *24*(1), 177–185.

Danecek, P., Bonfield, J. K., Liddle, J., Marshall, J., Ohan, V., Pollard, M. O., Whitwham, A., Keane, T., McCarthy, S. A., Davies, R. M. & Li, H. (2021). Twelve years of SAMtools and BCFtools. *GigaScience*, *10*(2), giab008.

Davies, B. S. J., Fong, L. G., Yang, S. H., Coffinier, C. & Young, S. G. (2009). The Posttranslational Processing of Prelamin A and Disease. *Annual Review of Genomics and Human Genetics*, *10*(1), 153–174.

Dittmer, T. A. & Misteli, T. (2011). The lamin protein family. *Genome Biology*, *12*(5), 222.

Dobin, A., Davis, C. A., Schlesinger, F., Drenkow, J., Zaleski, C., Jha, S., Batut, P., Chaisson, M. & Gingeras, T. R. (2012). STAR: ultrafast universal RNA-seq aligner. *Bioinformatics*, *29*(1), 15–21.

Dündar, F., Skrabanek, L. & Zumbo, P. (2019). *Introduction to differential gene expression analysis using RNA-seq*.

Eckersley-Maslin, M. A., Bergmann, J. H., Lazar, Z. & Spector, D. L. (2013). Lamin A/C is Expressed in Pluripotent Mouse Embryonic Stem Cells. *Nucleus*, *4*(1), 53–60.

Eriksson, M., Brown, W. T., Gordon, L. B., Glynn, M. W., Singer, J., Scott, L., Erdos, M. R., Robbins, C. M., Moses, T. Y., Berglund, P., Dutra, A., Pak, E., Durkin, S., Csoka, A. B., Boehnke, M., Glover, T. W. & Collins, F. S. (2003). Recurrent de novo point mutations in lamin A cause Hutchinson–Gilford progeria syndrome. *Nature*, *423*(6937), 293–298.

Evans, M. J. & Kaufman, M. H. (1981). Establishment in culture of pluripotential cells from mouse embryos. *Nature*, *292*(5819), 154–156.

Fülöp, N., Feng, W., Xing, D., He, K., Nőt, L. G., Brocks, C. A., Marchase, R. B., Miller, A. P. & Chatham, J. C. (2008). Aging leads to increased levels of protein O-linked N-acetylglucosamine in heart, aorta, brain and skeletal muscle in Brown-Norway rats. *Biogerontology*, *9*(3), 139.

Goldman, R. D., Shumaker, D. K., Erdos, M. R., Eriksson, M., Goldman, A. E., Gordon, L. B., Gruenbaum, Y., Khuon, S., Mendez, M., Varga, R. & Collins, F. S. (2004). Accumulation of mutant lamin A causes progressive changes in nuclear architecture in Hutchinson–Gilford progeria syndrome. *Proceedings of the National Academy of Sciences*, *101*(24), 8963–8968.

Gruenbaum, Y. & Foisner, R. (2015). Lamins: Nuclear Intermediate Filament Proteins with Fundamental Functions in Nuclear Mechanics and Genome Regulation. *Annual Review of Biochemistry*, *84*(1), 1–34.

Halim, A., Westerlind, U., Pett, C., Schorlemer, M., Rüetschi, U., Brinkmalm, G., Sihlbom, C., Lengqvist, J., Larson, G. & Nilsson, J. (2014). Assignment of Saccharide Identities through Analysis of Oxonium Ion Fragmentation Profiles in LC–MS/MS of Glycopeptides. *J. Proteome Res.*, *13*(12), 6024–6032.

Hamczyk, M. R., Villa-Bellosta, R., Quesada, V., Gonzalo, P., Vidak, S., Nevado, R. M., Andrés-Manzano, M. J., Misteli, T., López-Otín, C. & Andrés, V. (2019). Progerin accelerates atherosclerosis by inducing endoplasmic reticulum stress in vascular smooth muscle cells. *EMBO Molecular Medicine*, *11*(4), EMMM201809736.

Hart, G. W. & Copeland, R. J. (2010). Glycomics Hits the Big Time. *Cell*, *143*(5), 672–676.

Hart, G. W., Housley, M. P. & Slawson, C. (2007). Cycling of O-linked β-N-acetylglucosamine on nucleocytoplasmic proteins. *Nature*, *446*(7139), 1017–1022.

Hasper, J., Welle, K., Swovick, K., Hryhorenko, J., Ghaemmaghami, S. & Buchwalter, A. (2023). Long lifetime and tissue-specific accumulation of lamin A/C in Hutchinson–Gilford progeria syndrome. *Journal of Cell Biology*, *223*(1), e202307049.

Hrit, J., Goodrich, L., Li, C., Wang, B.-A., Nie, J., Cui, X., Martin, E. A., Simental, E., Fernandez, J., Liu, M. Y., Nery, J. R., Castanon, R., Kohli, R. M., Tretyakova, N., He, C., Ecker, J. R., Goll, M. & Panning, B. (2018). OGT binds a conserved C-terminal domain of TET1 to regulate TET1 activity and function in development. *ELife*, *7*, e34870.

Jung, H.-J., nier, C. C., Choe, Y., Beigneux, A. P., Davies, B. S. J., Yang, S. H., II, R. H. B., Hong, J., Sun, T., Pleasure, S. J., Young, S. G. & Fong, L. G. (2012). Regulation of prelamin A but not lamin C by miR-9, a brain-specific microRNA. *PNAS*, *109*.

Keembiyehetty, C., Love, D. C., Harwood, K. R., Gavrilova, O., Comly, M. E. & Hanover, J. A. (2015). Conditional Knock-out Reveals a Requirement for O-Linked N-Acetylglucosaminase (O-GlcNAcase) in Metabolic Homeostasis*. *Journal of Biological Chemistry*, *290*(11), 7097–7113.

Kim, B.-H., Chung, Y.-H., Woo, T.-G., Kang, S.-M., Park, S. & Park, B.-J. (2023). Progerin, an Aberrant Spliced Form of Lamin A, Is a Potential Therapeutic Target for HGPS. *Cells*, *12*(18), 2299.

Koch, A. J. & Holaska, J. M. (2014). Emerin in health and disease. *Seminars in Cell & Developmental Biology*, *29*, 95–106.

Kreppel, L. K., Blomberg, M. A. & Hart, G. W. (1997). Dynamic Glycosylation of Nuclear and Cytosolic Proteins CLONING AND CHARACTERIZATION OF A UNIQUE O-GlcNAc TRANSFERASE WITH MULTIPLE TETRATRICOPEPTIDE REPEATS*. *Journal of Biological Chemistry*, *272*(14), 9308–9315.

Lee, K. K., Haraguchi, T., Lee, R. S., Koujin, T., Hiraoka, Y. & Wilson, K. L. (2001). Distinct functional domains in emerin bind lamin A and DNA-bridging protein BAF. *Journal of Cell Science*.

Levine, Z. G. & Walker, S. (2016). The Biochemistry of O-GlcNAc Transferase: Which Functions Make It Essential in Mammalian Cells? *Annual Review of Biochemistry*, *85*(1), 631–657.

Liao, Y., Smyth, G. K. & Shi, W. (2014). featureCounts: an efficient general purpose program for assigning sequence reads to genomic features. *Bioinformatics*, *30*(7), 923–930.

Lin, C.-H., Liao, C.-C., Chen, M.-Y. & Chou, T.-Y. (2021). Feedback Regulation of O-GlcNAc Transferase through Translation Control to Maintain Intracellular O-GlcNAc Homeostasis. *International Journal of Molecular Sciences*, *22*(7), 3463.

López-Otín, C., Blasco, M. A., Partridge, L., Serrano, M. & Kroemer, G. (2013). The Hallmarks of Aging. *Cell*, *153*(6), 1194–1217.

Love, M. I., Huber, W. & Anders, S. (2014). Moderated estimation of fold change and dispersion for RNA-seq data with DESeq2. *Genome Biology*, *15*(12), 550.

Lubas, W. A., Frank, D. W., Krause, M. & Hanover, J. A. (1997). O-Linked GlcNAc

    Transferase Is a Conserved Nucleocytoplasmic Protein Containing Tetratricopeptide

    Repeats*. *Journal of Biological Chemistry*, *272*(14), 9316–9324.

Lunde, I. G., Aronsen, J. M., Kvaløy, H., Qvigstad, E., Sjaastad, I., Tønnessen, T.,

    Christensen, G., Grønning-Wang, L. M. & Carlson, C. R. (2012). Cardiac O-GlcNAc

    signaling is increased in hypertrophy and heart failure. *Physiological Genomics*,

    44(2), 162–172.

Maduro, C., Hoon, B. de & Gribnau, J. (2016). Fitting the Puzzle Pieces: the Bigger

    Picture of XCI. *Trends in Biochemical Sciences*, *41*(2), 138–147.

Marin, H., Simental, E., Allen, C., Martin, E., Panning, B., Al-Sady, B. & Buchwalter, A.

    (2024). The nuclear periphery confers repression on H3K9me2-marked genes and

    transposons to shape cell fate. *BioRxiv*, 2024.07.08.602542.

Martin, E. A., Maynard, J. C., Hrit, J., Augspurger, K., Picard, C. L., Feng, S., Jacobsen,

    S. E., Burlingame, A. L. & Panning, B. (2021). A dose-sensitive OGT-TET3 complex

    is necessary for normal Xist RNA distribution and function. *BioRxiv*,

    2021.06.19.449113.

Martin, G. R. (1981). Isolation of a pluripotent cell line from early mouse embryos

    cultured in medium conditioned by teratocarcinoma stem cells. *Proceedings of the*

    National Academy of Sciences, *78*(12), 7634–7638.

Martin, M. (2011). Cutadapt removes adapter sequences from high-throughput sequencing reads. *EMBnet.Journal*, *17*(1).

Martin, S. E. S., Tan, Z.-W., Itkonen, H. M., Duveau, D. Y., Paulo, J. A., Janetzko, J., Boutz, P. L., Törk, L., Moss, F. A., Thomas, C. J., Gygi, S. P., Lazarus, M. B. & Walker, S. (2018). Structure-Based Evolution of Low Nanomolar O-GlcNAc Transferase Inhibitors. *Journal of the American Chemical Society*, *140*(42), 13542–13545.

Maynard, J. C. & Chalkley, R. J. (2021). Methods for Enrichment and Assignment of N-Acetylglucosamine Modification Sites. *Molecular & Cellular Proteomics*, *20*, 100031.

Mlynarczyk-Evans, S., Royce-Tolland, M., Alexander, M. K., Andersen, A. A., Kalantry, S., Gribnau, J. & Panning, B. (2006). X Chromosomes Alternate between Two States prior to Random X-Inactivation. *PLoS Biology*, *4*(6), e159.

Nabet, B., Roberts, J. M., Buckley, D. L., Paulk, J., Dastjerdi, S., Yang, A., Leggett, A. L., Erb, M. A., Lawlor, M. A., Souza, A., Scott, T. G., Vittori, S., Perry, J. A., Qi, J., Winter, G. E., Wong, K.-K., Gray, N. S. & Bradner, J. E. (2018). The dTAG system for immediate and target-specific protein degradation. *Nature Chemical Biology*, *14*(5), 431–441.

Oca, R. M. de, Lee, K. K. & Wilson, K. L. (2005). Binding of Barrier to Autointegration Factor (BAF) to Histone H3 and Selected Linker Histones Including H1.1*. *Journal of Biological Chemistry*, *280*(51), 42252–42262.

Östlund, C., Ellenberg, J., Hallberg, E., Lippincott-Schwartz, J. & Worman, H. J. (1999). Intracellular trafficking of emerin, the Emery-Dreifuss muscular dystrophy protein. *Journal of Cell Science*, *112*(11), 1709–1719.

Ozawa, R., Hayashi, Y. K., Ogawa, M., Kurokawa, R., Matsumoto, H., Noguchi, S., Nonaka, I. & Nishino, I. (2006). Emerin-Lacking Mice Show Minimal Motor and Cardiac Dysfunctions with Nuclear-Associated Vacuoles. *The American Journal of Pathology*, *168*(3), 907–917.

Ran, F. A., Hsu, P. D., Wright, J., Agarwala, V., Scott, D. A. & Zhang, F. (2013). Genome engineering using the CRISPR-Cas9 system. *Nature Protocols*, *8*(11), 2281–2308.

Randolph, L. N., Bao, X., Zhou, C. & Lian, X. (2017). An all-in-one, Tet-On 3G inducible PiggyBac system for human pluripotent stem cells and derivatives. *Scientific Reports*, *7*(1), 1549.

Samson, C., Petitalot, A., Celli, F., Herrada, I., Ropars, V., Du, M.-H. L., Nhiri, N., Jacquet, E., Arteni, A.-A., Buendia, B. & Zinn-Justin, S. (2018). Structural analysis of the ternary complex between lamin A/C, BAF and emerin identifies an interface disrupted in autosomal recessive progeroid diseases. *Nucleic Acids Research*, *46*(19), 10460–10473.

Schreiber, K. H. & Kennedy, B. K. (2013). When Lamins Go Bad: Nuclear Structure and Disease. *Cell*, *152*(6), 1365–1375.

Schulz, E. G., Meisig, J., Nakamura, T., Okamoto, I., Sieber, A., Picard, C., Borensztein, M., Saitou, M., Blüthgen, N. & Heard, E. (2014). The Two Active X Chromosomes in Female ESCs Block Exit from the Pluripotent State by Modulating the ESC Signaling Network. *Cell Stem Cell*, *14*(2), 203–216.

Shafi, R., Iyer, S. P. N., Ellies, L. G., O'Donnell, N., Marek, K. W., Chui, D., Hart, G. W. & Marth, J. D. (2000). The O-GlcNAc transferase gene resides on the X chromosome and is essential for embryonic stem cell viability and mouse ontogeny. *Proceedings of the National Academy of Sciences*, *97*(11), 5735–5739.

Shin, J.-Y. & J.Worman, H. (2021). Molecular Pathology of Laminopathies. *Annual Review of Pathology: Mechanisms of Disease*.

Simon, D. N., Wriston, A., Fan, Q., Shabanowitz, J., Florwick, A., Dharmaraj, T., Peterson, S. B., Gruenbaum, Y., Carlson, C. R., Grønning-Wang, L. M., Hunt, D. F. & Wilson, K. L. (2018). OGT (O-GlcNAc Transferase) Selectively Modifies Multiple Residues Unique to Lamin A. *Cells*, *7*(5), 44.

Spear, E. D., Alford, R. F., Babatz, T. D., Wood, K. M., Mossberg, O. W., Odinammadu, K., Shilagardi, K., Gray, J. J. & Michaelis, S. (2019). A humanized yeast system to analyze cleavage of prelamin A by ZMPSTE24. *Methods*, *157*, 47–55.

Stephen, H. M., Adams, T. M. & Wells, L. (2021). Regulating the Regulators: Mechanisms of Substrate Selection of the O-GlcNAc Cycling Enzymes OGT and OGA. *Glycobiology*, *31*(7), 724–733.

Tan, Z.-W., Fei, G., Paulo, J. A., Bellaousov, S., Martin, S. E. S., Duveau, D. Y., Thomas, C. J., Gygi, S. P., Boutz, P. L. & Walker, S. (2020). O-GlcNAc regulates gene expression by controlling detained intron splicing. *Nucleic Acids Research*, *48*(10), 5656–5669.

Trinidad, J. C., Barkan, D. T., Gulledge, B. F., Thalhammer, A., Sali, A., Schoepfer, R. & Burlingame, A. L. (2012). Global Identification and Characterization of Both O-GlcNAcylation and Phosphorylation at the Murine Synapse*. *Molecular & Cellular Proteomics*, *11*(8), 215–229.

Walgren, J. L. E., Vincent, T. S., Schey, K. L. & Buse, M. G. (2003). High glucose and insulin promote O-GlcNAc modification of proteins, including α-tubulin. *American Journal of Physiology-Endocrinology and Metabolism*, *284*(2), E424–E434.

Wang, C.-Y., Froberg, J. E., Blum, R., Jeon, Y. & Lee, J. T. (2017). Comment on "Xist recruits the X chromosome to the nuclear lamina to enable chromosome-wide silencing." *Science*, *356*(6343).

Zvetkova, I., Apedaile, A., Ramsahoye, B., Mermoud, J. E., Crompton, L. A., John, R., Feil, R. & Brockdorff, N. (2005). Global hypomethylation of the genome in XX embryonic stem cells. *Nature Genetics*, *37*(11), 1274–1279.

Publishing Agreement

It is the policy of the University to encourage open access and broad distribution of all theses, dissertations, and manuscripts. The Graduate Division will facilitate the distribution of UCSF theses, dissertations, and manuscripts to the UCSF Library for open access and distribution. UCSF will make such theses, dissertations, and manuscripts accessible to the public and will take reasonable steps to preserve these works in perpetuity.

I hereby grant the non-exclusive, perpetual right to The Regents of the University of California to reproduce, publicly display, distribute, preserve, and publish copies of my thesis, dissertation, or manuscript in any form or media, now existing or later derived, including access online for teaching, research, and public service purposes.

Katherine Augspurger

Author Signature

3/12/2025

Date